What the bubble knows: Lake methane dynamics revealed by sediment gas bubble composition

Article *in* Limnology and Oceanography · February 2019

DOI: 10.1002/lno.11133

4 authors:

Timon Langenegger
University of Geneva
5 PUBLICATIONS **16** CITATIONS
SEE PROFILE

Dominic Vachon
Umeå University
33 PUBLICATIONS **732** CITATIONS
SEE PROFILE

Daphne Donis
University of Geneva
33 PUBLICATIONS **251** CITATIONS
SEE PROFILE

Daniel Frank McGinnis
University of Geneva
171 PUBLICATIONS **4,228** CITATIONS
SEE PROFILE

LIMNOLOGY and OCEANOGRAPHY

ASLO

Limnol. Oceanogr. 9999, 2019, 1–19

doi: 10.1002/lno.11133

What the bubble knows: Lake methane dynamics revealed by sediment gas bubble composition

T. Langenegger ,* **D. Vachon** ,[a] **D. Donis** , **D. F. McGinnis** *

Aquatic Physics Group, Faculty of Science, Department F.-A. Forel for Environmental and Aquatic Sciences (DEFSE), University of Geneva, Geneva, Switzerland

Abstract

Atmospheric methane (CH_4) concentrations have more than doubled in the past ~ 250 yr, although the sources of this potent greenhouse gas remain poorly constrained. Freshwaters contribute ~ 20% of natural CH_4 emissions, about half attributed to ebullition. Estimates remain uncertain as ebullition is stochastic, making measurements difficult, time consuming, and costly with current methods (e.g., floating chambers, funnel gas traps, and hydroacoustics). We present a novel approach to quantify basin-wide hypolimnetic CH_4 fluxes at the sediment level based on measurements of bubble gas content and modeling of dissolved pore-water gases. We show that the relative ebullition flux pathway can be resolved by knowledge of only bubble gas content. As sediment CH_4 production, diffusion, and ebullition are interrelated, the addition of a second observation allows closing the entire sediment CH_4 balance. Such measurements could include bubble formation depth, sediment diffusive fluxes, ebullition, sediment CH_4 production, or the hypolimnetic CH_4 mass balance. The measurement of bubble gas content is particularly useful for identifying local ebullitive hotspots and integrating spatial heterogeneity of CH_4 fluxes. Our results further revealed the crucial effect of water column depth, production rates, and hypolimnetic dissolved CH_4 concentrations on sediment CH_4 dynamics. Although we apply the model to cohesive sediments in an anoxic hypolimnion, the model can be applied to shallow, oxic settings by altering the CH_4 production rate curve to account for oxidation. Utilizing our approach will provide a deeper understanding of in-lake CH_4 budgets, and thus improve CH_4 emission estimates from inland freshwaters at the regional and global scales.

Atmospheric methane (CH_4) concentrations have more than doubled in the last 250 yr (Wuebbles and Hayhoe 2002). With a global warming potential 34 times higher than CO_2 over a 100 yr period (Myhre et al. 2013), CH_4 has come to renewed attention as atmospheric concentrations continue to rise after plateauing during the last decade (Dlugokencky et al. 2011; Nisbet et al. 2014). There is currently considerable uncertainty in the global atmospheric CH_4 budgets and the reasons behind the observed atmospheric CH_4 trends, highlighting the need to better understand the various sources and sinks (Kirschke et al. 2013; Turner et al. 2017; Worden et al. 2017). Lakes as natural sources of microbially produced CH_4 contribute about 20% of the natural emissions to the global budget (Bastviken et al. 2011). Approximately, half of these emissions are attributed to CH_4 ebullition; however, these estimates remain highly uncertain (Bastviken et al. 2011) as ebullitive emissions are notoriously difficult, time consuming, and costly to accurately quantify (Wik et al. 2016).

In freshwater sediments, significant quantities of biogenic CH_4 are naturally produced by microorganisms (methanogens) in the terminal process of anaerobic degradation of organic matter (Conrad 2005). Two main pathways are distinguished: acetoclastic methanogenesis utilizing acetate and hydrogenotrophic methanogenesis, which is based on the reduction of CO_2 with hydrogen (Conrad 2005). CH_4 production rates in sediments have been found to be dependent on the quality of organic matter, O_2 exposure, and temperature (Schulz and Conrad 1995; Sobek et al. 2012; Yvon-Durocher et al. 2014). Production rates generally decrease rapidly and near exponentially with sediment depth (Zepp Falz et al.

*Correspondence: timon.langenegger@unige.ch and daniel.mcginnis@unige.ch

[a]Present Address: Department of Ecology and Environmental Sciences, Umeå University, Umeå, Sweden

Additional Supporting Information may be found in the online version of this article.

1999; Popp et al. 2000; Wilkinson et al. 2015). If the net CH_4 production is higher than the diffusive transport from the sediment to the water, sediment pore-water dissolved gas concentrations will become oversaturated and bubbles are formed and may be released (Boudreau 2012; Schmid et al. 2017).

For pore-water bubble formation, it is necessary to consider the total dissolved gas pressure, which is the sum of the dissolved partial pressures of all sparingly soluble sediment gases (mainly CH_4 and nitrogen, N_2). Bubbles form when the total dissolved gas pressure becomes equal to or exceeds the local pressure (hydrostatic + atmospheric; Miyake 1951; D'Aoust 2007; *see* Fig. 1). Even though CO_2 is biologically produced in the sediment (Conrad 2005), total dissolved gas pressure is mainly driven by CH_4 as CH_4 is ~ 29 times less soluble than CO_2 (at 5°C) (Sander 2015). Accordingly, sediment bubbles contain little CO_2 and consist mainly of CH_4 and N_2 (Casper et al. 2000; Walter et al. 2008). The mechanics of formation, growth, and release of sediment bubbles (ebullition) depend on physical properties of the sediments (Boudreau 2012; Katsman et al. 2013; Liu et al. 2016, 2018; Scandella et al. 2016) and changes in local pressure and bottom shear stress (Casper et al. 2000; Joyce and Jewell 2003).

Ebullitive release of sediment gas is highly variable in space and time (DelSontro et al. 2015). Consequently, considerable efforts are required to obtain accurate estimates for whole-lake emissions (Natchimuthu et al. 2016). CH_4 ebullition is typically measured using floating chambers (Bastviken et al. 2004), with hydroacoustic methods (Ostrovsky et al. 2008) or with gas trap funnels (DelSontro et al. 2010; Delwiche et al. 2015; Wilkinson et al. 2015). These conventional approaches have several limitations. First, due to the stochastic nature of ebullition, a large number of measurement sites are required to obtain accurate estimates representative for a whole lake. With gas trap funnels, for example, Wik et al. (2016) recommended 39 measurements of ebullition at 11 or more locations, which then provides an unbiased estimation of ebullition. Second, both gas trap funnel and hydroacoustic methods rely on the knowledge of CH_4 fraction in bubble gas to determine CH_4 ebullitive rates. Even though it is possible to analyze the CH_4 content in trapped bubble gas, measurements may be biased due to gas exchange with the water column and potential CH_4 oxidation. Finally, no method is available that integrates all components needed for a mechanistic understanding of sediment CH_4 mass balance (consisting of production, diffusion, and ebullition). To overcome these challenges, we propose a novel approach based on modeling of dissolved pore-water gases combined with knowledge of CH_4 bubble content to improve basin-wide CH_4 dynamics, including ebullitive emission estimates.

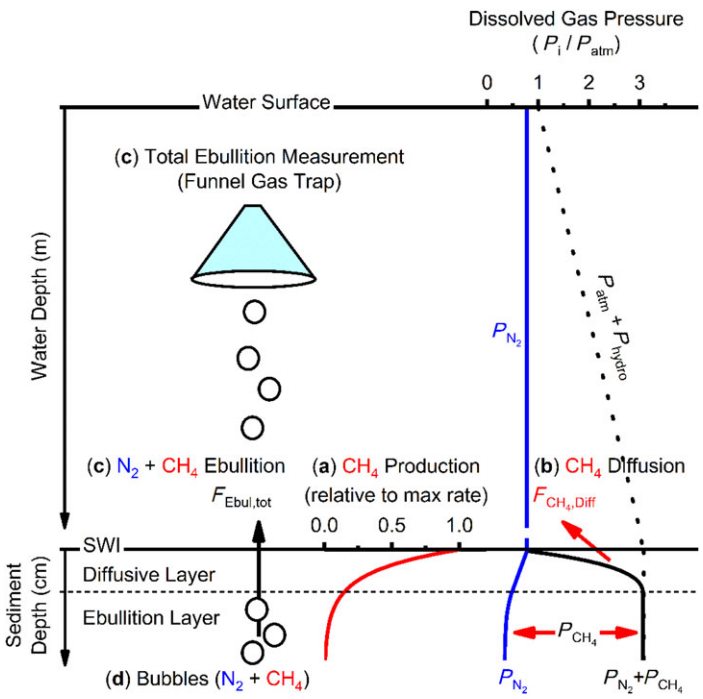

Fig. 1. Schematic of CH_4 processes for pore-water mass balance model with the ebullition model based on Bazhin (2003, 2010). (a) Sediment CH_4 production, (b) CH_4 diffusion flux $F_{CH_4,Diff}$ at SWI, (c) total ebullition flux $F_{Ebul,tot}$ at the SWI, and (d) composition of sediment bubble gas. P_i is the dissolved gas partial pressure of a given gas.

Several authors have demonstrated that CH_4 ebullition deprives pore water of other gases, some of which would otherwise reflect atmospheric saturation concentrations (e.g., N_2 and noble gases; Reeburgh 1969; Martens and Berner 1977; Kipphut and Martens 1982; Chanton et al. 1989; Brennwald et al. 2005). Reeburgh (1969) investigated dissolved gases in sediments from active ebullition sites and found profiles of N_2 and argon (Ar) to be depleted with respect to concentrations at the sediment–water interface (SWI). The author attributed the phenomenon to bubbles transporting both CH_4 and other pore-water dissolved gases (i.e., N_2 and noble gases) out of the sediment (Reeburgh 1969; Brennwald et al. 2005). This effect, which Reeburgh (1969) termed "stripping," is primarily dependent on ebullition rate and water column depth. Both Martens and Berner (1977) and Kipphut and Martens (1982) estimated ebullition rates by inverse modeling of pore-water profiles of dissolved N_2 and Ar. In agreement with the stripping hypothesis, Chanton et al. (1989) observed that at higher ebullition rates, the bubble gas leaving the sediment contained less N_2 and more CH_4. Chanton et al. (1989) suggested that this information could be useful for estimating ebullitive fluxes.

More recently, Bazhin (2003, 2010) developed a steady state theory for dissolved pore-water gases in sediments with active CH_4 ebullition, which has been verified in the laboratory by Kusmin et al. (2006). Bazhin (2003, 2010) introduced an upper diffusive layer below the SWI where bubbles do not form since the total dissolved gas pressure does not reach oversaturation. The model is driven entirely by sediment CH_4 production, which can be parameterized by an exponential decay. From the exponential fit of sediment CH_4 production

with depth, the model calculates the thickness of the diffusive layer, pore-water profiles of dissolved CH_4 and N_2, CH_4 diffusive and ebullitive fluxes, and finally the bubble gas composition (i.e., content of CH_4 and N_2; *see* Fig. 1). The model of Bazhin (2003, 2010) has two degrees of freedom. Therefore, the state of the system, including the complete sediment CH_4 mass balance, can be determined from two given independent observations (discussed below).

CH_4 produced in the sediment (Fig. 1) can exit via diffusion and ebullition. In a steady state situation, the mass balance at the sediment level is given by net production = diffusion + ebullition. In this study, we present an inverse modeling approach that utilizes this relationship combined with sediment bubble gas composition (Fig. 1d) to estimate CH_4 pathways in the small, eutrophic kettle lake, Lake Soppen (aka Soppensee).

Specially, we apply a sediment pore-water model and show that:

- With reasonable assumptions, the fraction of the produced CH_4 leaving the sediment either as ebullition or diffusion can be predicted with only knowledge of the bubble CH_4 content and the water depth where the bubble was collected.
- With the addition of any additional independent observation (below), the complete sediment CH_4 mass balance can be resolved.

The additional observation can be any of the following: (1) point ebullition estimates, (2) depth of sediment-bubble formation, (3) a well-resolved sediment CH_4 production profile, or (4) CH_4 diffusive flux. Given the same measurement effort, traditional methods (i.e., funnels, hydroacoustics, surface chambers, micrometeorological, open path optical, and infrared camera systems) combined with our approach provide significantly improved estimates of whole-lake CH_4 dynamics.

Methods

Study site

Lake Soppen (aka Soppensee) is a small, glacially formed kettle lake in Buttisholz (Canton Lucerne) in the Swiss plateau at an elevation of 596 m above sea level. It has a surface area of 0.227 km^2, a maximal and mean depth of 26 and 12.3 m (Fig. 2; Lotter 1989). Given the small catchment area of 1.6 km^2 and a mean annual outflow of 0.03 $m^3\ s^{-1}$ through a small stream in the north, Fischer (1996) estimated the maximum residence time of the water to be 3.1 yr. The lake is eutrophic and lies in an area of intense agriculture. The sediments in the top 6 m are authigenic, fine-grained cohesive, and rich in organic carbon, whereas below 6 m, glacially deposited clays are found (Lotter 1991; Fischer 1996). From the observed depletion of dissolved noble gases in the sediment pore water (down to 7 m), Brennwald et al. (2005) estimated that the lake sediments have been releasing CH_4 bubbles for the past centuries.

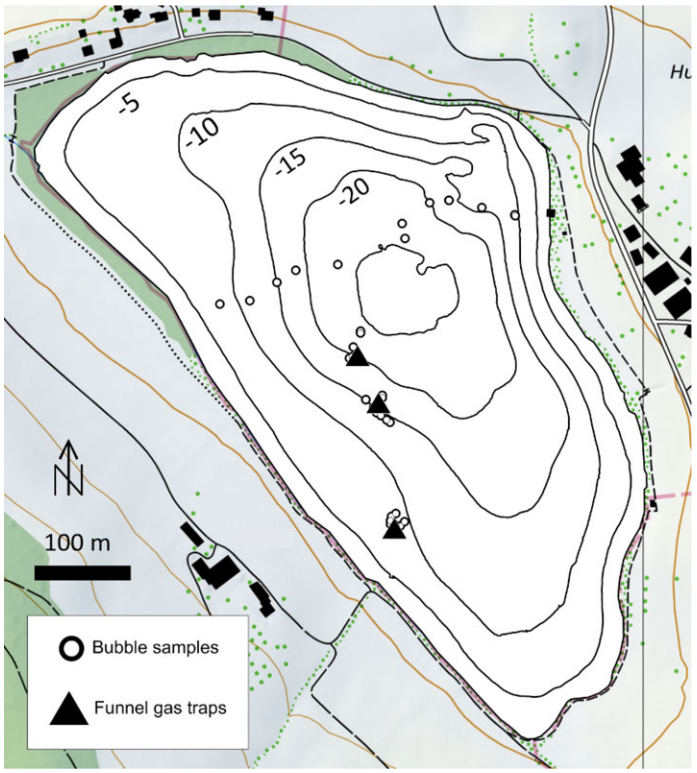

Fig. 2. Bathymetric map of Lake Soppen (Soppensee, Buttisholz, Switzerland) with sampling locations.

The lake was monitored from April 2016 to December 2017 for CH_4 and water column properties, including temperature, O_2, and CH_4 in the water column (*see* Supporting Information section S1 and example profile in Supporting Information Fig. S1). In summer, water temperature reaches 24–26°C in the surface mixed layer, whereas temperatures remain close to 5°C in the bottom waters below 10 m water depth. During the stratified periods, the lake water becomes entirely anoxic below ~ 8 m, whereas dissolved CH_4 concentrations increase rapidly below 10 m, becoming as high as 1.3 mol m^{-3} at the bottom of the lake in autumn 2017.

Sediment CH_4 flux estimates and measurements

We quantify the three components of the steady state sediment CH_4 mass balance: (1) sediment CH_4 production, (2) diffusive CH_4 flux at the SWI, and (3) ebullitive CH_4 flux at the SWI. Sediment CH_4 production was measured from the increase of CH_4 in incubation vials filled with sediment subsamples from four cores taken at water depths 8, 20, and 26 m on the 20 July 2016 and 26 m water depth on the 01 March 2016 (*see* Supporting Information Figs. S2–S5 and Tables S1–S3). As in situ and incubation temperatures were slightly different, we applied a temperature correction based on the data of Nozhevnikova et al. (2007) (*see* Supporting Information

Fig. S6). The sediment incubation methods followed the procedure by Wilkinson et al. (2015) and are detailed in the Supporting Information section S2.

Diffusive CH_4 fluxes at the SWI were calculated from pore-water measurements of cores sampled from various depths in 2016 and 2017. The measurements followed the methods of Donis et al. (2017) and are described in details in the Supporting Information section S3. Briefly, a cut syringe method was applied and head space gas was analyzed on a Cavity Ring-down Spectrometer (Model Picarro G2201-i), which provided both pore-water CH_4 concentration and $\delta^{13}C_{CH_4}$ values (the Picarro instrument came with factory calibration and a comparison with a brand-new instrument [same model] showed excellent agreement for the $\delta^{13}C_{CH_4}$ values). Diffusive CH_4 fluxes at the sediment–water interface were then calculated according to Fick's first law (*see* Supporting Information Fig. S7 and Table S4).

Total ebullitive and CH_4 ebullitive fluxes at the SWI were measured with inverted funnel gas traps at three locations in the lake with water depths 10, 15, and 21 m (*see* Fig. 2). The funnels were installed above the sediment at 4 m below the water surface and captured gas bubbles released from the sediment. With the bubble model of McGinnis et al. (2006), we subsequently corrected fluxes for gas exchange during the rise of bubbles from the SWI to the funnel gas trap and thus obtained rates of total gas ebullition and CH_4 ebullition at the SWI. We show ebullition rates from the period July to December 2017, during which data are available for all the three funnel sites (*see* Supporting Information section S4 and Table S5).

Sediment bubble gas sampling, composition, and origin

We collected bubble gas samples from the sediments within ~ 5 m of the funnel sites and along a transect (*see* Fig. 2). The sampler consisted of a funnel with a weight attached underneath (i.e., at the wide part) and a glass crimp vial (50 or 120 mL) attached to the top (see Supporting Information section S5 and sketch of sampling device in Supporting Information Fig. S8). To sample the bubble gas, the device was filled with lake water and lowered to the sediments. The sediment was impacted ~ 15 times with the weight to completely fill the vial with gas. When the sampling device was retrieved to lake surface, the vial was capped (polytetrafluoroethylene-coated butyl rubber) and crimped under water. Sample vials were kept submerged in lake water until measurement within 1 d.

The composition of the gas samples (CH_4, CO_2, N_2, and O_2) was determined with a field portable mass spectrometer (*see* Brennwald et al. [2016] and Supporting Information section S6 and Table S6). We measured the stable carbon isotopic signature ($\delta^{13}C_{CH_4}$) of bubble gas samples on the same Picarro stable isotope analyzer used for pore-water analysis. Samples were diluted to concentrations in the range of the stable isotope analyzer (< 500 ppm) by injecting 50 μL of bubble gas using a 0.5-mL gas-tight glass syringe (SGE Analytical Science) into a 120 mL sealed glass vial containing artificial air (no CH_4 or CO_2, Carbagas). After injection of the sample, an additional 60 mL of artificial gas was injected into the 120 mL glass vial, with another 60 mL syringe inserted to relieve the pressure. The two inserted 60-mL all-glass syringes (Poulten Graf Fortuna Optima) were then used to mix the gas in the 120 mL vial by alternatively pressing and releasing the plungers. This was done five times to ensure adequate mixing.

The sediment depth of bubble origin was estimated based on the assumption that the $\delta^{13}C_{CH_4}$ of the dissolved pore-water CH_4 should match the $\delta^{13}C_{CH_4}$ of the bubble gas CH_4. For this, we calculated the average $\delta^{13}C_{CH_4}$ pore-water profile obtained between 8–13 m (n = 5) and 18–26 m water depth (n = 5) and took their average for the depth range between 13 and 18 m water depth (no pore-water profiles were measured in that depth range). We subsequently utilized these $\delta^{13}C_{CH_4}$ profiles to infer the bubble origin depth from $\delta^{13}C_{CH_4}$ of the sediment bubble gas as shown for an example in Supporting Information Fig. S9 and section S7.

Sediment modeling

Model introduction

Our modeling approach largely follows the theory of dissolved gases in sediment pore water as described in Bazhin (2003, 2010). The model describes the concentrations of dissolved gases CH_4 and N_2 (and potentially other gases) in the sediment pore water (see overview in Fig. 3). Except for CH_4, which is produced, the pore-water dissolved gas concentration profiles are assumed to be exclusively driven by molecular diffusion and transport of stripped pore-water gases out of the sediment by ebullition (i.e., bubble stripping). The profiles of dissolved gas concentration are assumed to be in steady state and that no further gas transport occurs across the bubble surface once the bubble moves from its depth of origin. As in Bazhin (2003, 2010), the upper sediment diffusive layer, where theoretically no ebullition occurs, is defined where the total dissolved gas pressure is lower than the local (atmospheric + hydrostatic) pressure (Fig. 3).

The model development is described in the next section, with the key variables listed in Table 1 and the principle assumptions summarized below. The principle assumptions should be considered when applying the model; we revisit the major assumptions in the discussion.

- Conceptualization with upper nonebullitive layer (diffusion layer) and lower ebullition layer (*see* Bazhin 2010 and assumptions therein).
- Dissolved pore-water concentration profiles are in steady state and the average seasonal effect of intermittent ebullition on pore-water dissolved gas concentrations and fluxes can be modeled by considering an average seasonal ebullition rate in the steady state model.
- Bubbles in the sediments are in local equilibrium with the dissolved pore-water gases (*see* Brennwald et al. 2005,

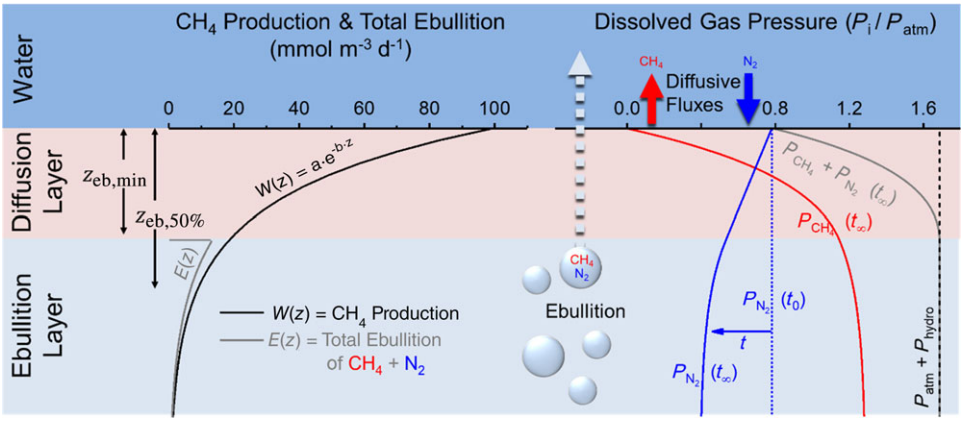

Fig. 3. Sketch of steady state sediment model based on Bazhin (2003, 2010). CH_4 production $W(z)$ leads to ebullition in the lower ebullition layer, where the total dissolved gas pressure from N_2 + CH_4 is equal to the local pressure. N_2 is continuously removed from the sediment due to stripping in the lower ebullition layer, while it is resupplied to the sediment pore water from the SWI. Gas concentrations are constant at the SWI, and fluxes are zero at the base of the sediment.

Table 1. Summary of input and output variables.

Variable	Description	Typical units
Inputs		
a	Sediment CH_4 production rate per bulk volume at SWI (Eq. 2)	mmol m^{-3} d^{-1}
b	Exponential decay of sediment CH_4 production rate per bulk volume with sediment depth z (Eq. 2)	m^{-1}
Outputs		
$C_i(z)$	Dissolved gas profiles in the sediment (Eq. 1)	mmol m^{-3}
$F_{CH_4,D}$	Diffusive flux of CH_4 at the SWI (Eq. 9)	mmol m^{-2} d^{-1}
$F_{CH_4,E}$	Ebullition flux of CH_4 leaving the sediment (Eq. 10)	mmol m^{-2} d^{-1}
$F_{tot,E}$	Total gas ebullition flux (see text below Eq. 12)	mmol m^{-2} d^{-1}
f_E	CH_4 ebullition fraction of production (Eq. 11)	–
X_{CH_4}	Bubble CH_4 fraction (Eq. 12)	–
$z_{eb,min}$	Sediment depth at which ebullition starts (Eq. 4)	m
$z_{eb,50\%}$	Sediment depth at which 50% of integrated total ebullition flux is reached (Eq. 8)	m

section 3.1). Other than gas removal (stripping), we do not consider other physical effects of bubbles in the sediment or their release (i.e., no bubble-mediated pore-water advection; *see* Flury et al. 2015). We assume that bubbles leaving the sediment do not interact notably with the surrounding sediment and pore water while leaving the sediment (i.e., no additional mass transfer once they begin to exit the sediment).

- Advective transport is not considered (i.e., only cohesive sediments are considered).
- Bioturbation is not explicitly considered.
- CH_4 is the only gas produced in the sediments, i.e., no N_2 production (Kipphut and Martens 1982; Martens et al. 1998; Wilkinson et al. 2015; Schmid et al. 2017).
- Boundary conditions: At the SWI, the concentrations of dissolved pore-water gas are equal to the concentrations in the lake and N_2 is in equilibrium with the atmosphere. At the bottom of the sediment, a zero flux condition is applied.

Transport and reaction equations

The transport equations in our model of dissolved concentrations $C_i(z)$ of gases i in the sediment pore water are written in summarized form in Eqs. 1a and 1b. Transport processes are different for the upper nonebullitive region (Eq. 1a; sediment depth $z \le z_{eb,min}$) and the lower ebullitive region (Eq. 1b; $z > z_{eb,min}$; *see* Fig. 3): In the upper nonebullitive region, diffusive transport (first term, Fick's second law) and production (second term, $W_i(z)$) are in equilibrium, whereas in the ebullition layer, an additional third term for the loss of gas due to bubble stripping is added. This additional stripping term is the local total ebullition rate $E(z)$ multiplied by the individual gas mole fraction at sediment depth z. Although we only consider CH_4 and N_2, the transport equations for any dissolved gas i can be described in the following equation.

$$\varphi \cdot D_i \cdot \frac{\partial^2 C_i(z)}{\partial z^2} + W_i(z) = 0, \quad 0 < z \le z_{eb,min} \tag{1a}$$

$$\varphi \cdot D_i \cdot \frac{\partial^2 C_i(z)}{\partial z^2} + W_i(z) - E(z) \cdot \frac{K_{H,i} \cdot C_i(z)}{P} = 0, \quad z > z_{eb,min} \tag{1b}$$

where φ is the sediment porosity (–), D_i is the effective molecular diffusion (D_m) corrected for tortuosity ($D_i = \theta^{-2} D_{i,m}$; Boudreau 1997), C_i is dissolved concentration (mol m^{-3}), E is total gas ebullition per bulk volume (mol m^{-3} d^{-1}), W_i the gas production per bulk volume (mol m^{-3} d^{-1}), K_H is Henry's law volatility constant (Pa m^3 mol^{-1}), and P is the local critical gas

pressure (Pa). We measured porosity φ (*see* Supporting Information section S8 and Fig. S10) and applied a constant measured value of $\varphi = 0.9$, and therefore for tortuosity, following Boudreau (1997), a value of $\theta^2 = 1 - \ln(\varphi^2) = 1.2$. Temperature-dependent molecular diffusion coefficients $D_{i,\mathrm{m}}$ were obtained by piecewise linear interpolation of the data presented by Jähne et al. (1987), and Henry's law volatility constants $K_{\mathrm{H},\,i}$ were calculated at in situ temperature according to the parameterization presented by Sander (2015). The local critical gas pressure P is calculated as $P = \rho g h + P_{\mathrm{atm}} - P_{\mathrm{H_2O}}$, with the water density ρ = 1000 kg m^{-3}, gravity g = 9.81 m s^{-2}, the water depth h in (m), the atmospheric pressure P_{atm}, which is ~ 944 hPa at Lake Soppen, and the temperature-dependent water vapor saturation pressure $P_{\mathrm{H_2O}}$ calculated with the equation of Buck (1981).

The model (Eq. 1) is driven by the production of gases $W_i(z)$ (mol m^{-3} d^{-1}). In this study, we consider no production of N_2 ($W_{\mathrm{N_2}} = 0$), and CO_2 contributes negligible amounts to gas pressure (not modeled). We apply an exponential profile of CH_4 production rate per bulk volume ($W_{\mathrm{CH_4}}$) as a function of sediment depth z:

$$W_{\mathrm{CH_4}}(z) = a \cdot e^{-b \cdot z} \tag{2}$$

where a is the maximum CH_4 production (mmol CH_4 m^{-3} d^{-1}) at the upper-most layer of sediment and b is the decay parameter (m^{-1}).

Ebullition layer condition *E*

Within the lower ebullition layer (Fig. 3), the total dissolved gas pressure is equal to the hydrostatic plus atmospheric pressure minus water vapor saturation pressure (Eq. 3).

$$K_{\mathrm{H,CH_4}} \cdot C_{\mathrm{CH_4}}(z) + K_{\mathrm{H,N_2}} \cdot C_{\mathrm{N_2}}(z) = P = \rho g h + P_{\mathrm{atm}} - P_{\mathrm{H_2O}} \tag{3}$$

Bubbles are assumed to be formed only below a sediment depth $z_{\mathrm{eb,\,min}}$ where the total dissolved gas pressure reaches local oversaturation. The two regions are described by a different set of differential equations (see Eq. 1). At the interface, concentrations and fluxes are continuous (Bazhin 2010). Before any pore-water concentrations $C_i(z)$ can be modeled, the extent of each region (i.e., $z_{\mathrm{eb,\,min}}$) must be found. The depth $z_{\mathrm{eb,\,min}}$ is defined by the combination of Eqs. 1–3. From this it follows that at $z = z_{\mathrm{eb,\,min}}$, the depth where bubbles start to form, the condition in Eq. 4 must be met (Bazhin 2010 the derivation of Eq. 4 is provided in Supporting Information section S9).

$$0 = 1 - z_{\mathrm{eb,min}} \cdot b \cdot e^{-z_{\mathrm{eb,min}} \cdot b} - e^{-z_{\mathrm{eb,min}} \cdot b} - b^2 \cdot \frac{D_{\mathrm{CH_4}}}{a \cdot K_{\mathrm{CH_4}}} \cdot (P_{\mathrm{res}}) \tag{4}$$

In Eq. 4, P_{res} is introduced to simplify the equation and is the local atmospheric + hydrostatic pressure minus the partial pressures of gases at the SWI, which decreases with the lake water CH_4 concentration $C_{\mathrm{CH_4,lake}}$:

$$P_{\mathrm{res}} = \rho g h + P_{\mathrm{atm}} - P_{\mathrm{H_2O}} - 0.78 \cdot P_{\mathrm{atm}} - K_{\mathrm{H,CH_4}} C_{\mathrm{CH_4,lake}} \tag{5}$$

The depth $z_{\mathrm{eb,\,min}}$ can be found numerically from Eq. 4. Note that, in general, $z_{\mathrm{eb,\,min}}$ is dependent on the gases that are produced/consumed and on how the production is distributed (see Supporting Information section S9). In this work, Eq. 4 is valid for only CH_4 production, which decays exponentially with depth (*see* Eq. 2). Equation 4 is used both to determine the value of $z_{\mathrm{eb,\,min}}$ and whether bubbles can be formed, i.e., if $z_{\mathrm{eb,\,min}}$ is shallower than the total sediment depth (L), then bubbles are formed, otherwise bubbles are not formed.

Boundary conditions

At the bottom of the sediment $z = L$, a zero-flux condition is set for all gases, $\frac{\partial C_i}{\partial z}(z = L) = 0$. The position of the lower boundary was set at L = 5 m, as we found that results did not change significantly for $L > 5$ m. At the SWI ($z = 0$), the CH_4 concentration is assumed to be equal to the concentration of the overlying lake water. The dissolved partial pressure of N_2 is assumed independent of water depth and therefore fixed at the SWI to a value of $0.78 P_{\mathrm{atm}}$ (see measurements by Horn et al. [2017]).

Interestingly, the N_2 boundary conditions imply a lower limit to the amount of CH_4 in bubbles. Assuming negligible N_2 production, the dissolved gas pressure of N_2 is limited to a maximum of $0.78 P_{\mathrm{atm}}$. As bubble gas consists mainly of N_2 and CH_4 (Casper et al. 2000; Walter et al. 2008; see also our own results), the main contribution to dissolved partial gas pressure comes from these two gases, and other gases can be neglected. Considering that the required minimum total dissolved gas pressure for bubble formation increases linearly with water depth (Eq. 3; Fig. 1), then it follows that the minimum dissolved partial pressure of CH_4 required for bubble formation also increases linearly with depth. Therefore, the minimum CH_4 fraction in a sediment bubble in equilibrium with the pore water as a function of water depth h is described as:

$$X_{\mathrm{CH_4,\,min}} = 1 - (0.78 \cdot P_{\mathrm{atm}}) / (P_{\mathrm{atm}} + \rho \cdot g \cdot h) \tag{6}$$

Solution properties

Equations 1–4 are solved numerically for the concentration profile $C_i(z)$. Besides concentration profiles, the below-defined solution properties are calculated as outputs (see summary key variables Table 1).

From the combination of Eqs. 1 and 3, the total bulk gas ebullition rate with sediment depth $E(z)$ (mmol m^{-3} d^{-1}) is defined as

$$E(z) = \varphi \left(D_{\mathrm{N_2}} \frac{\partial^2 C_{\mathrm{N_2}}(z)}{\partial z^2} + D_{\mathrm{CH_4}} \frac{\partial^2 C_{\mathrm{CH_4}}(z)}{\partial z^2} \right) + W_{\mathrm{CH_4}}(z) \tag{7}$$

Additionally, from this ebullition rate profile $E(z)$ (Eq. 7), we can derive the sediment depth $z_{eb,50\%}$ above which 50% of the depth-integrated ebullition occurs.

$$\frac{\int_0^{z_{eb,50\%}} E(z)\,dz}{\int_0^{L} E(z)\,dz} = 0.5 \quad (8)$$

Diffusive fluxes $F_{i,D}$ (mmol m^{-2} d^{-1}) of dissolved gases at the SWI are defined with Fick's first law

$$F_{i,D} = \varphi D_i \frac{\partial C_i}{\partial z}(z=0) \quad (9)$$

Integrating the production rate (Eq. 2) simplifies the total production to $\int W(z) = ab^{-1}$ (mmol m^{-2} d^{-1}). The ebullition flux of CH_4 ($F_{CH_4,E}$) is then production – diffusion

$$F_{CH_4,E} = \frac{a}{b} - F_{CH_4,D} \quad (10)$$

and the CH_4 ebullition pathway fraction f_E of total production is

$$f_E = 1 - \frac{F_{CH_4,D}}{a/b} \quad (11)$$

Finally, the CH_4 bubble composition X_{CH_4} is given as a ratio of the CH_4 ebullitive flux divided by total gas ebullitive flux

$$X_{CH_4} = \frac{F_{CH_4,E}}{F_{N_2} + F_{CH_4,E}} \quad (12)$$

note that $F_{N_2} = -F_{N_2,D} = F_{N_2,E}$, as for steady state, the bubble transport of N_2 gas out of the sediment must equal the diffusive flux back to the sediment (no N_2 production; *see* Eq. 1). Also note that in Eq. 12, the denominator is the total ebullition gas flux, i.e., $F_{tot,E} = F_{N_2} + F_{CH_4,E}$. The total ebullition gas flux can also be written as $F_{tot,E} = F_{CH_4,E}/X_{CH_4}$. In the upper diffusive layer (Fig. 3), CH_4 production is balanced by loss from the sediment due to molecular diffusion. For an overview of processes, see Fig. 3.

Overview model inputs and outputs variables

A summary of the input variables that drive the model and output variables are given in Table 1 and are summarized in Fig. 3. In the general model, a and b are known inputs (Eq. 2) and the remaining variables are solved. Using an inverse modeling approach (discussed below), any two parameters from Table 1 need to be known to solve for the remaining variables (except for the combination of f_E and X_{CH_4}, which are not independent as we show in the results).

Solving for the output variables in Table 1, an example of a model solution for 5°C, 20 m water depth, and zero lake CH_4 concentration is shown in Fig. 3. Gas concentrations are constant at the SWI and fluxes are zero at the bottom end of the sediment. Ebullition $E(z)$ of N_2 + CH_4 is fuelled by CH_4 production $W(z)$ and occurs only in the ebullition layer where the total dissolved gas pressure of N_2 + CH_4 is equal to the local pressure. While N_2 is continuously removed from the sediment via exiting bubbles, it is diffusively resupplied from the SWI. As we assume that no significant N_2 is produced in the sediments, dissolved concentration of N_2 decrease linearly within the diffusive layer, in contrast to CH_4, which is produced according to $W(z)$. The model is solved with MATLAB boundary value problem solver *bvp4c*. Note that the model can be easily adapted to track additional gases, e.g., including a production term for N_2 or N_2O, which may be significant in some systems (Higgins et al. 2008; Baulch et al. 2011). For code description and possible adaptions, see Supporting Information section S10 and example scripts (available via e-mail). See Supporting Information Figs. S11 and S12 for inclusion of N_2 production.

Inverse modeling approaches for CH_4 fluxes

For a given water depth and temperature, the model is driven by the generally a priori unknown two sediment production parameters a and b, which makes the model a system with two degrees of freedom. However, for any pair of observations known in Table 1, a unique pair of a and b can be found such that the two given observations are precisely matched by the model. If an assumption on either parameter a or b can be made, then only one additional observation of any of the parameters on Table 1 must be known to determine the remaining unknown parameters. Furthermore, as shown by Bazhin (2010), for any accurately measured dissolved gas sediment profile, it is possible to find the solution for a and b and all the remaining parameters listed in Table 1. We used the MATLAB global minimum search routine *fmincon* to find the solutions for fitting given observations (see description of code in Supporting Information section S10 and example scripts, available via e-mail).

Applied approaches to resolve CH_4 fluxes

Although there are many combinations of observations that can be investigated for resolving the CH_4 mass balance, we explore the following approaches based on our measured data. All these approaches utilize the bubble CH_4 composition (fulfilling one of the two required observations).

Approach 1: From three deployed funnel gas traps (Fig. 2) and nearby sediment gas samples, we have observations of ebullition flux at the SWI and bubble CH_4 content (described below). Given these two observations, the parameters a and b and the complete sediment CH_4 mass balance are resolved with inverse modeling.

In this approach, we assume that the gas sampled around the funnels reflects the mean ebullition flux of that funnel. To avoid disturbing the sediment just below the funnel, we

sampled bubble gas in the immediate vicinity, thus the depths at which the samples were obtained slightly varied from the funnel depth. As hydrostatic pressure has a major impact on ebullition (West et al. 2016), we linearly interpolated ebullition rates between the funnels at 15 and 20 m. The depth around the 10 m funnel did not vary much, so the bubble samples were collected close to 10 m depth.

Approach 2: For the transect sediment gas samples (Fig. 2), the ebullition fluxes are not known. It is, however, possible to estimate $z_{eb,50\%}$ from measurements of the isotopic signature $\delta^{13}C_{CH_4}$ of both the bubble gas and the sediment pore-water dissolved CH_4. With this additional indirect observation of $z_{eb,50\%}$ combined with the measured CH_4 bubble content, it is also possible to estimate the CH_4 mass balance using the inverse modeling.

Approach 2 is based on the idea that isotope measurements are a good method for determining the average sediment depth at which bubbles originate and thus a good estimate for either $z_{eb,min}$ or $z_{eb,50\%}$ in the model. Basically, the measured bubble $\delta^{13}C_{CH_4}$ is assumed to be the same as the dissolved pore-water $\delta^{13}C_{CH_4}$ where the bubble was formed. Consequently, the corresponding isotope ratio from the sediment profile gives an approximate depth where the bubble was formed. As previously discussed, we used the averaged $\delta^{13}C_{CH_4}$ pore-water profiles from three depth ranges (Supporting Information section S7). For approach 2, we assume that these averaged profiles are representative throughout the lake (within the defined water depth ranges).

Approach 3: It is also possible to assume a value for the CH_4 production parameters a or b (Eq. 2). Here, we propose to assume either a or b as found from the application of approach 1 nearby the funnel sites and assume the selected value applies to the entire lake. Then, with additional bubble gas content data collected on the transect, we can estimate the CH_4 mass balance at the locations where the samples were collected.

Sediment area-weighted average fluxes

Finally, using these approaches, we estimate the whole-lake hypolimnetic (below 8 m) CH_4 production and sediment CH_4 fluxes. With different approaches 1–3, we obtained flux estimates of CH_4 ebullition, diffusion, and production for each sediment gas sample collected over a range of depths. From these, we can extrapolate the hypolimnetic basin-wide CH_4 flux estimates using the sediment-area–weighted averaged fluxes according to

$$F_{\text{avg}} = \frac{\sum_i \Delta A_{sed,i} \cdot F_i}{A_{\text{sed,total}}} \quad (13)$$

$\Delta A_{\text{sed},i}$ is the sediment fraction in 0.5 m intervals (Δz = 0.5 m) at depth water z_i multiplied by the linearly interpolated flux F_i at that depth.

Results

We present results of direct estimates of the sediment CH_4 mass balance consisting of production rates (from sediment incubations), diffusive fluxes at SWI (from pore-water profiles), and ebullition (from funnel gas trap). Furthermore, we present measured composition and sediment bubble gas and inferred sediment depth of bubble origin. Using these data, we then show the model results for the sediment CH_4 mass balance using our three approaches. We provide model results at the bubble gas sampling locations as well as integrated results for estimates of the basin-scale hypolimnetic CH_4 budget.

Result I—Observations

Net sediment CH_4 production rates

Laboratory incubations of sediments were performed to estimate potential sediment CH_4 production. Figure 4 shows that net production rates decline rapidly within the first ~ 10 cm in the sediments (see also Supporting Information Tables S1 and S2 and section S2). Following the assumption that profiles could be described by exponential decay (Eq. 2), we found parameter a ranging from 129 to 502 mmol CH_4 m^{-3} d^{-1} (mean a = 239 mmol CH_4 m^{-3} d^{-1}) and parameter b ranging from 10.1 to 43 m^{-1} (mean b = 30 m^{-1}; *see* Supporting Information Table S3). Integrated production rates corresponding to fitted a and b (Prod = a/b) range between 3.2 and 12.8 mmol CH_4 m^{-2} d^{-1} (black solid circles in Fig. 5).

Diffusive and ebullitive CH_4 fluxes at the sediment–water interface

Diffusive CH_4 fluxes at the SWI were estimated with Fick's first law (see Supporting Information section S3). The individual pore-water profiles of dissolved CH_4 and $\delta^{13}C_{CH_4}$ and estimated local diffusive fluxes at the SWI are summarized on Supporting Information Fig. S7. Resolved diffusive fluxes where bin averaged and were (mean ± 1 SD) 9.2 ± 1.7 mmol m^{-2} d^{-1} at 12 m water depth (n = 4) and 16.6 ± 11.4 mmol m^{-2} d^{-1} at 25 m water depth (n = 5; Fig. 5; Supporting Information Table S4).

Total gas ebullition fluxes (i.e., CH_4 + N_2) at the SWI were measured using deployed funnels gas traps at three sites (10, 15, and 21 m water depths). We corrected the data for dissolution and measured CH_4 bubble gas fraction (*see* Supporting Information section S4). This resulted in average estimated CH_4 ebullitive fluxes from July to December 2017 of 2.5 ± 1.0, 0.57 ± 0.12, and 1.2 ± 0.4 mmol CH_4 m^{-2} d^{-1} for the funnels at 10, 15, and 21 m, respectively (Fig. 5). For temporal dynamics, see Supporting Information section S4 and Table S5.

Composition and origin of bubble gas

We sampled sediment gas bubbles in situ with the sediment pore-water gas sampler described in the Methods section and Supporting Information section S5. Samples consisted mainly of CH_4 and N_2, which make up on average

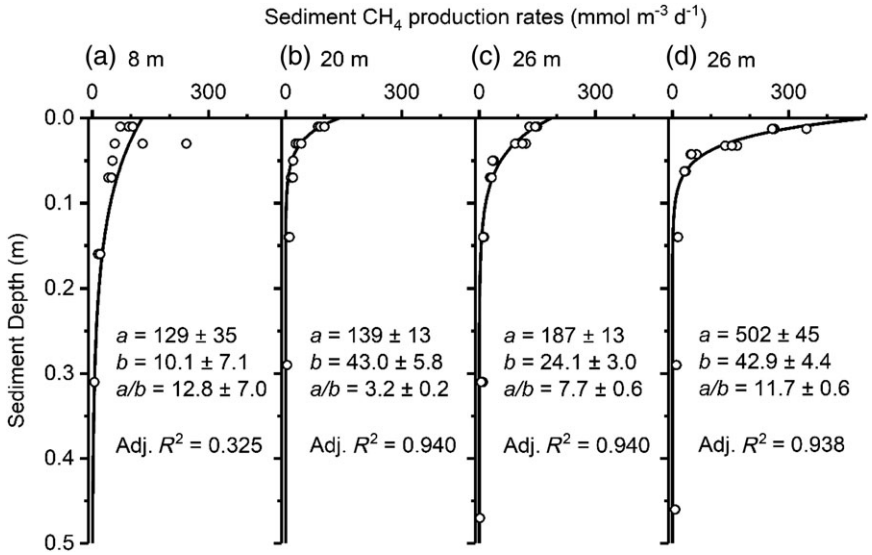

Fig. 4. Incubation results for CH_4 production rates as measured in laboratory sediment incubations for (**a**) core 8 m, (**b**) core 20 m, (**c**) core 26 m (1), and (**d**) core 26 m (2). Assuming exponential production (Eq. 2), the best-fitting parameters a and b and the derived depth-integrated production Prod = a/b are given as value ± standard error as well as the adjusted R^2 of the exponential fit. For data, see also Supporting Information Tables S1 and S3 and Figs. S2–S5.

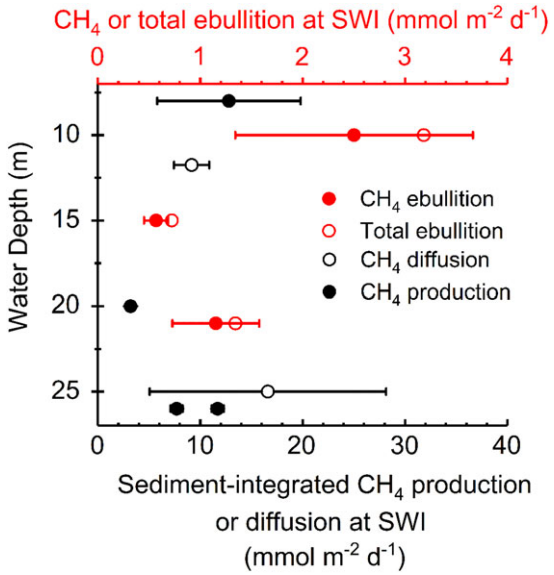

Fig. 5. Summary of integrated production rates from Fig. 4, and CH_4 diffusive and CH_4 ebullitive fluxes at the SWI. Error bars show standard deviation for ebullition and standard errors from parameter fitting for production.

98.9% of the bubble gases, while CO_2 contributed only 0.77% and O_2 was present only in trace amounts (see data in Supporting Information Table S6 and section S6). Figure 6a shows that the samples at locations near the funnel sites (colored symbols) and from the transect (open symbols) all contain more CH_4 than the theoretical minimum CH_4 fraction $X_{CH_4,min}$ defined by Eq. 6. Samples from the transect generally had higher CH_4 fractions than samples nearby funnel sites at the same water depth. Additionally, we have analyzed $\delta^{13}C_{CH_4}$ of sediment gas samples and found values in the range of −74‰ to −66.5‰ (Fig. 6b; Supporting Information Table S6). Samples from the transect generally had higher stable isotope ratios (i.e., less negative) than samples nearby the funnel sites (Fig. 6c).

To determine depth of origin of the sampled bubble gas, we measured the $\delta^{13}C_{CH_4}$ of pore-water dissolved CH_4 (see pore-water profiles in Supporting Information Fig. S7 and section S3). Figure 6d shows the average $\delta^{13}C_{CH_4}$ for pore-water profiles obtained between 8 and 13 m water depth (n = 5) and 18–26 m water depth (n = 5). We took the averages of these profiles for the depth range between 13 and 18 m. In general, the profiles of all $\delta^{13}C_{CH_4}$ were consistently lower (more negative) with sediment depth z (Fig. 6d and Supporting Information Fig. S7). These data are used to infer the depth of origin of sampled sediment-released bubbles (Fig. 6c) by matching the bubble $\delta^{13}C_{CH_4}$ isotope values (Fig. 6b) with the corresponding $\delta^{13}C_{CH_4}$ from the pore-water profile (Fig. 6d). An example of the estimation of sediment depth of bubble origin from $\delta^{13}C_{CH_4}$ is shown in Supporting Information Fig. S9 and section S7.

Result II—Modeling sediment CH_4 fluxes

Estimating CH_4 ebullition pathway

We demonstrate that, with the model, we can estimate the proportion of the CH_4 transport pathways, i.e., the relative amount of CH_4 production leaving the sediment as ebullition, with simply the knowledge of bubble gas CH_4 content (Eqs. 11 and 12; Fig. 6a). As a first step in our modeling exercise, we developed the contour

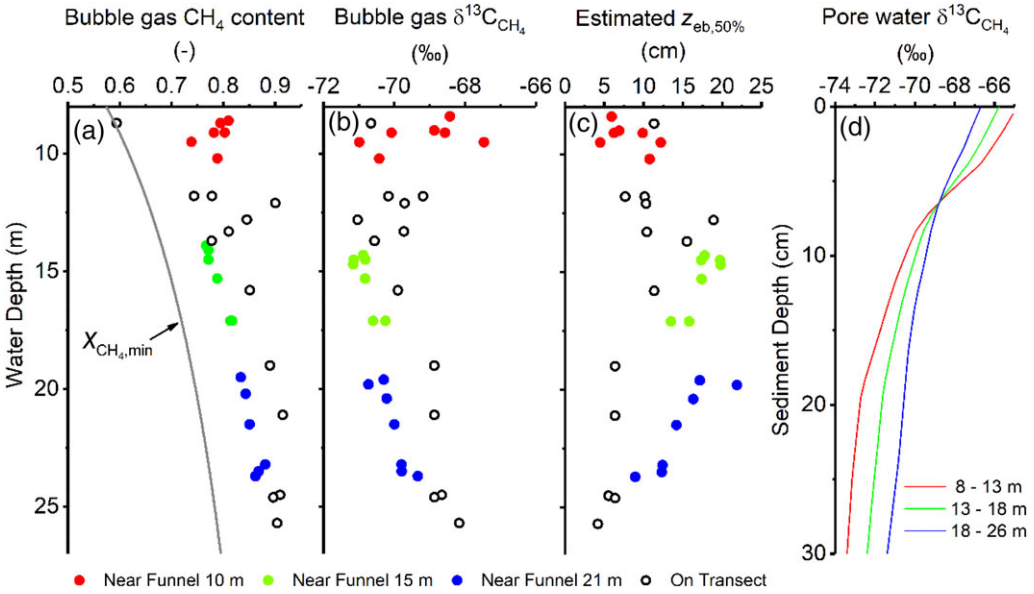

Fig. 6. (**a**) CH_4 fraction of sampled sediment-released bubbles. Gray solid line represents theoretical minimum CH_4 fraction of bubbles as a function of depth (see text). (**b**) $\delta^{13}C_{CH_4}$ isotopes measured in sediment gas. (**c**) Estimated sediment-depth origin of sampled sediment gas inferred from bubble gas $\delta^{13}C_{CH_4}$ (**b**) and (**d**) averaged pore-water dissolved $\delta^{13}C_{CH_4}$ profiles.

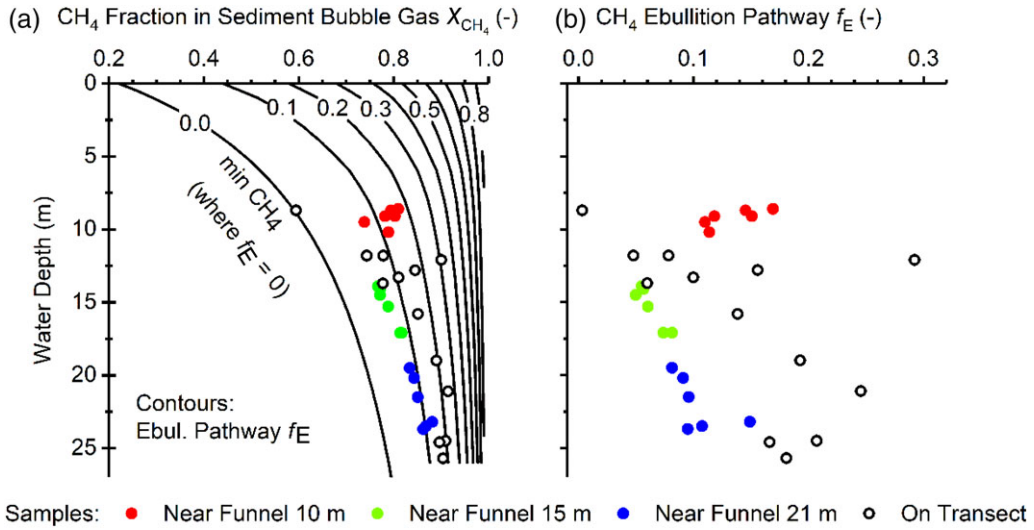

Fig. 7. (**a**) Contour lines of ebullition pathway calculated for representative water temperature and dissolved CH_4 profile measured on the 28 and 29 August 2017. The proportion of ebullition pathway relative to the total CH_4 production can be determined from bubble gas CH_4 fraction and water depth. Also shown is the minimum possible CH_4 fraction, which is dependent on water depth only and coincides with zero ebullition. (**b**) Ebullition pathway corresponding to measured bubble CH_4 fraction (Fig. 6a) calculated for exact individual temperatures and lake water dissolved CH_4.

shown on Fig. 7a. We ran the model from 0 to 26 m depth at 1 m interval varying a and b (i.e., production a/b) in Eq. 1 from a = 1–1500 mmol m^{-3} d^{-1} and b = 5–70 m^{-1}. The model was run using the temperature and dissolved CH_4 profiles shown on Supporting Information Fig. S1.

By running all combinations, we see that for a given depth the proportion of the total CH_4 production emitted via ebullition f_E (see Eq. 11) is directly related to the bubble composition X_{CH_4} (Eq. 12). This pathway f_E has a single solution for a given bubble CH_4 fraction at a given depth. Therefore, the ebullition pathway can be estimated in every case simply with knowledge of the bubble CH_4 fraction and vice versa. As an example, Fig. 7a shows contour lines of the ebullition proportion of total production f_E, which is only dependent on the water column depth and bubble CH_4 fraction X_{CH_4} (Eq. 12) overlain with the points of measured bubble CH_4 fraction from Fig. 6a. Therefore, for a constant water depth, an increase in bubble CH_4 content corresponds to an increase in the

proportion of the ebullition pathway. Similarly, for a fixed-bubble CH_4 content X_{CH_4}, the ebullition pathway decreases with increasing water depth. Figure 7a also shows the theoretical minimum CH_4 fraction (Eq. 6) which coincides with the contour of zero ebullition pathway and is independent of temperature. Figure 7b shows the exact ebullition pathway proportion corresponding to measured bubble CH_4 fraction, calculated at local water temperature and dissolved CH_4 concentration.

Estimating complete sediment CH_4 balance

We have shown that it is possible to estimate the CH_4 ebullition pathway f_E (Eq. 11) based on measured bubble CH_4 fraction alone X_{CH_4} (Eq. 12). However, this approach gives no quantitative information on production or flux magnitudes. For estimates of CH_4 ebullition, diffusive flux and production, additional observations are required. To do this, we have applied the three approaches described in the Methods section.

Figure 8 shows the inverse modeling results based on fitting the measured sediment bubble CH_4 content at different sampling locations in the lake and from different estimation approaches. Therefore, all the modeling results shown in Fig. 8 reproduce exactly the measured bubble gas CH_4 content previously presented in Fig. 6a. For each model calculation, the sum of CH_4 ebullition flux (Fig. 8a) and CH_4 diffusive flux at the SWI (Fig. 8b) are equal to the integrated sediment CH_4 production (Fig. 8c). The ratio of CH_4 ebullition flux (Fig. 8a) over the integrated sediment CH_4 production (Fig. 8c) is equal to the ebullition pathway previously presented in Fig. 7b. Figure 8d shows the modeled sediment depth of bubble origin $z_{eb,50\%}$. Each of the approaches are detailed and compared to each other in the following section (Fig. 9).

Approach 1

For this approach, we use data from the three sites with funnel gas traps 10, 15, and 21 m, where we have measurements of ebullition fluxes at the SWI (Fig. 5) and CH_4 content in bubble gas sampled nearby the funnels (Fig. 6a). We used a linear interpolation to infer ebullitive fluxes between the 15 and 21 m funnels. Again, we assume that the ebullition flux measured at the 10 m funnel is representative for gas samples collected in the immediate vicinity of the funnel. We therefore use the inverse modeling approach with CH_4 ebullition rate and bubble gas content to infer the CH_4 production parameters a and b (Eq. 2) and thus solve for the total sediment CH_4 mass balance (i.e., production, diffusion, and ebullition) and depth of ebullition layer $z_{eb,50\%}$ (Fig. 8). This approach is then compared to approach 2 below (Fig. 9).

Approach 2

Approach 2 is based on our idea that the sediment depth of bubble origin inferred from bubble and pore-water isotope measurements (Fig. 5c) is a good proxy for $z_{eb,50\%}$ in the model, that is, the sediment depth above which 50% of the depth-integrated ebullition occurs. Approach 2 was applied to both sediment bubble gas samples from nearby the funnel sites and on the transect (Fig. 8). Briefly, approach 2 uses CH_4 bubble content and the isotope estimated $z_{eb,50\%}$ to estimate parameters a and b, and thus solve the complete mass balance (Fig. 8a–d). We compare the estimates for ebullition (Fig. 9a)

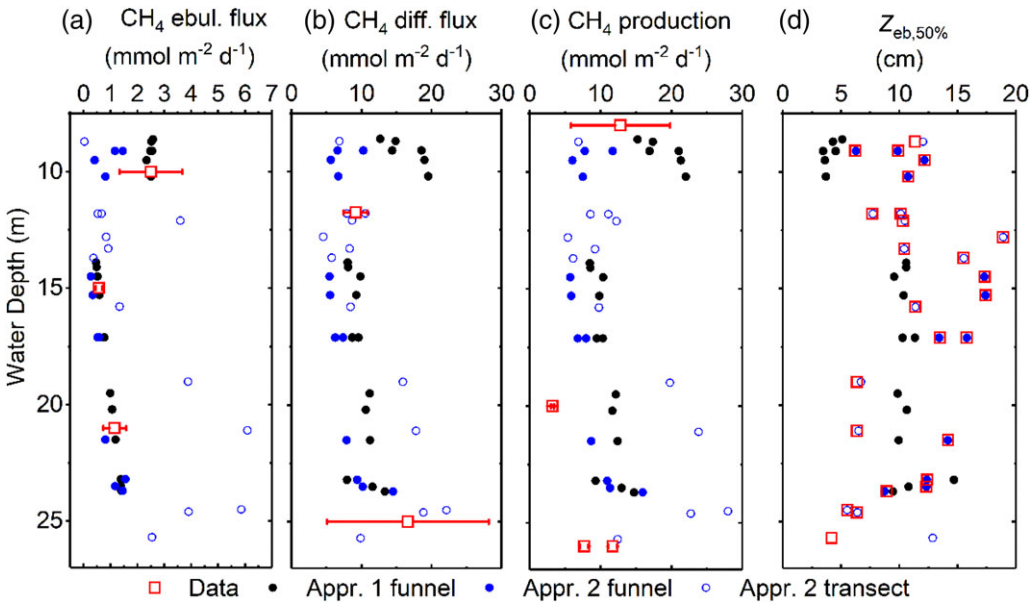

Fig. 8. Modeling results (**a**–**d**) based on measured sediment bubble gas CH_4 content at different sampling locations (near funnel are solid, transects are open symbols) for approaches 1 and 2. Open red square symbols in (**a**–**c**) are measured data as in Fig. 5 and in (**d**), red squares were obtained from matching $\delta^{13}C_{CH_4}$ of bubbles and pore-water profiles. In (**a**), error bars show standard deviation of measured CH_4, in (**b**) standard deviation of binned diffusive fluxes, and in (**c**) standard error of production from exponential fit of incubations.

and diffusion (Fig. 9d) from approach 1 to those obtained with approach 2 for the near-funnel data where we have measured ebullition.

Approach 3

To infer the total sediment mass balance from sediment bubble gas composition, it is possible to assume a value for either parameter *a* (approach 3a) or parameter *b* (approach 3b; Eq. 2) based on the measured sediment CH_4 production rates (Fig. 4). However, *a* (surface production rate) or *b* (depth-decay parameter) can also be estimated with approach 1 (combination of ebullition and bubble gas data). This has the advantage of fitting simpler parameters with a priori assumption of total production rate. Here, as we did not measure ebullition on the transect, we assume a value for either parameter *a* (approach 3a) or parameter *b* (approach 3b; Eq. 2) from approach 1 and apply these for the transect data.

For samples near the 15 and 21 m funnel, the estimated parameters *a* and *b* were similar to each other, whereas the 10 m funnel was somewhat different (*see* Supporting Information Fig. S13). For samples nearby the 15 and 21 m, we found a mean value for parameter *a* of 295.1 mmol m^{-2} d^{-1} and a mean value for parameter *b* of 27.1 m^{-1}. Both values are in the same order of magnitude as inferred from sediment incubations (Fig. 4), and we subsequently use those values for approach 3. In Fig. 9, we compare the ebullition and flux estimates from approaches 3a and 3b with approach 2 for the transect data.

Integrating estimated CH_4 fluxes to the lake basin

The results from the approaches 1, 2, 3a, and 3b are area-weighted averaged and integrated over the entire lake basin below 8 m water depth as basin-scale fluxes (Table 2).

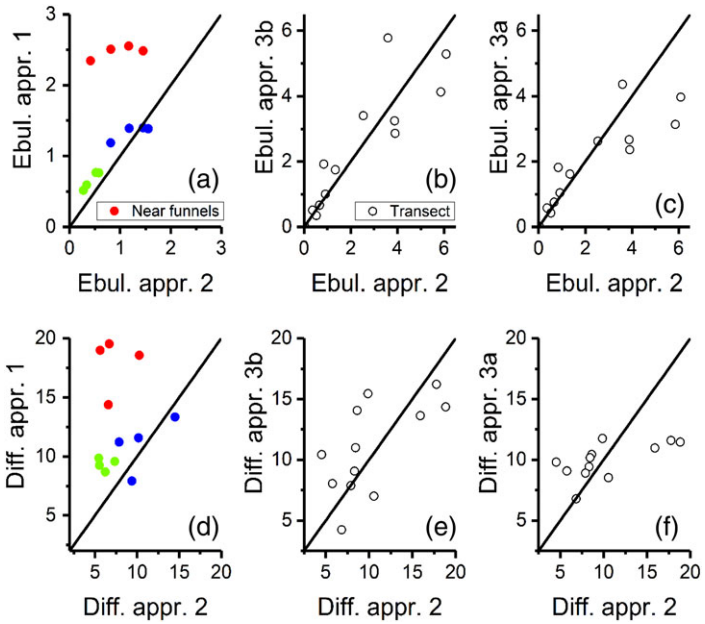

Fig. 9. Comparison of CH_4 ebullition fluxes (**a**–**c**) and CH_4 diffusive fluxes (**d**–**f**) in mmol m^{-2} d^{-1} from different estimation approaches 1, 2, 3a, and 3b at the different sampling locations. Symbols: Red, green, and blue are data collected near the 10, 15, and 21 m funnels, respectively, and open symbols are transect data (Fig. 2).

Discussion

We present a modeling approach to estimate sediment CH_4 production and flux pathways based on relatively easy-to-collect field data. The basis of the approach is the fact that gas bubbles alter the pore-water dissolved gas concentrations and that the sediment bubble gas content reflects the intensity of ebullition (Chanton et al. 1989). As a reminder, our key assumptions for this approach are: (1) the system is in steady state, (2) exponential decay rates of production (although this can be changed), and (3) results represent fluxes over a seasonal scale.

Estimating CH_4 pathways from bubble CH_4 content

As shown on Fig. 6a, the theoretical minimum CH_4 content (negligible ebullition fluxes) of a bubble can be expressed as a function of depth. Based on Eq. 6, the minimum bubble CH_4 content must increase with depth and is only a function of total pressure (independent of CH_4 source but assuming no significant production of N_2 or gases other than CH_4 and bubbles in equilibrium). Approaching greater depths, the CH_4 bubble content asymptotically approaches 100% of the total bubble gas content. For example, at 100 m depth, the

Table 2. Overview of sediment area-weighted CH_4 flux and production estimates from different locations and estimation approaches for the hypolimnion.

	Ebullition at SWI (mmol CH_4 m^{-2} d^{-1})	Diffusion at SWI (mmol CH_4 m^{-2} d^{-1})	Integrated production (mmol CH_4 m^{-2} d^{-1})
Approach 1 (near funnels)	1.5	12.7	14.2
Approach 2 (near funnels)	0.8	7.9	8.7
Approach 2 (transect)	2.1	10.9	12.9
Approach 2 (all results)	1.4	9.4	10.8
Approach 3a (transect)	1.6	9.5	11.2
Approach 3b (transect)	2.0	10.2	12.1

minimum fraction of bubble CH_4 must be greater than 93%, whereas at 1000 m depth, the minimum CH_4 fraction in a bubble must be 99.2% (neglecting other potential biologically produced gases). As ebullition rates increase, however, CH_4 content is altered. For example, at a fixed depth in a lake, the higher the ebullition rate, the higher the bubble CH_4 content becomes and the greater the fraction of the total CH_4 production emitted as ebullition (Fig. 7b).

Therefore, a major finding of this work is that by knowing the CH_4 bubble content and the water depth at which it was collected, the proportion between diffusive and ebullitive flux pathways can be estimated (Fig. 7b). It is also apparent from Fig. 7b that the resolution of this approach decreases with increasing depth. This means that as the depth increases, the uncertainty of our inverse modeling approaches also increases. All the collected bubble gas content data (except a single point) were in excess of the minimum CH_4 content predicted by Eq. 6 (*see* Figs. 6a, 7a). We can therefore infer that ebullition was ongoing at every sampling site, and at every site, we could thus quantify the fraction of production emitted as ebullition.

Using only the gas bubble composition is useful for finding local emission hotspots, lake basin-wide emission variability, and relative ebullition flux rates (Fig. 7); however, it does not give any quantitative information on the CH_4 production or fluxes. Combined with a basin-scale hypolimnetic CH_4 mass balance (e.g., Schmid et al. (2017)), the ebullition and diffusive fluxes can be easily determined. If a second parameter, together with bubble gas content, or any two parameters shown in Table 1 are determined, then the hypolimnetic lake CH_4 mass balance and flux pathways can be estimated with very good approximation (note that the combination of f_E and X_{CH_4} are not independent and need a third parameter).

Comparison of the inverse modeling approaches

Approach 1 fit the model to observations of bubble gas CH_4 content and total ebullition flux at SWI collected with in situ bubble gas traps. We found that the samples nearby the funnels 15 and 21 m with a mean value for parameter a of 295.1 mmol m^{-2} d^{-1} and a mean value for parameter b of 27.1 m^{-1} were comparable to the values found from sediment incubations (Fig. 4). However, the fitted parameters a and b for samples nearby the 10 m funnel fell out of this range, with parameter a above 500 mmol CH_4 m^{-3} d^{-1} and b over 40 m^{-1}. This can also be observed on Fig. 9a,b when comparing to the results from approach 2.

Although overall agreement with the measured data is very good (Fig. 8), we speculate that the differences observed at the 10 m site might be due to locally enhanced sediment CH_4 production rates or may be an artifact due to the inappropriate selection of physical parameters (temperature, porosity, and tortuosity) used for this method. As this site is the shallowest, it is more exposed to changing seasonal temperature and dissolved oxygen in the overlying water. Also, we cannot rule out an influence of potential N_2 production at this funnel site (for effect of N_2 production on bubble gas composition and pore-water profiles; *see* Supporting Information Figs. S11 and S12). Finally, a limitation of approach 1 is that it can only be applied around the areas where the ebullition data were collected.

Approach 2 is particularly interesting as all the three sediment CH_4 parameters (ebullition, diffusion, and production) are resolved entirely with independent measurements, i.e., bubble CH_4 content and bubble depth of origin. This is based on our presented hypothesis that the bubble depth of origin can be inferred with the combination of the bubble $\delta^{13}C_{CH_4}$ value with the corresponding depth of the matching $\delta^{13}C_{CH_4}$ value in the pore water (Fig. 6b–d). This means that approach 2 can potentially be applied to quantify the CH_4 production and flux pathways without using funnel gas traps.

CH_4 production and flux estimates from approach 2 agree extremely well with data collected at all depths (Fig. 8) and also with estimates from approach 1 for depths below 10 m (Figs. 8a–c, 9a,d). This finding also suggests that this is a robust approach to apply to the transect data. Comparing the funnel-only estimates from approach 2 with the transect-only estimates, we conclude that ebullition along the transect is up to 2–3 times higher than nearby the funnel sites, whereas diffusion about 1.2 times and production 1.3 times higher on the transect (*see* Table 2; Fig. 8). These results highlight both the location of relative hotspots and the need for extensive spatial coverage for accurate basin-scale estimates of CH_4 production and flux pathways.

Approaches 3a and 3b were applied using the mean values of parameters a and b (Eq. 2) obtained from modeling data (approach 1) based on samples collected around the 15 and 21 m funnel. Both approaches agreed well with approach 2 (Table 2), however, approach 3b matched better. If funnel traps are deployed, then approaches 3a and 3b only need additional data for bubble gas composition from different locations. Thus, spatial variability of fluxes and hotspots can be estimated quickly and cost effectively. If we take approach 2 as a baseline for comparison (Fig. 9), approach 3b (where we assume a basin-wide constant decay rate of production) appears to give more consistent estimates than approach 3a (where we assume basin-wide constant maximum surface production). This makes sense, as approach 3a only assumes the shape of the production curve rather than values of surface production (a) (discussed below).

Modeling basin-scale CH_4 production and flux pathways

We scale our results to provide the basin-wide model-inferred hypolimnetic CH_4 budget (Table 2). We want to point out the differences in the estimates using only the funnels vs. the more robust estimate of including the transect data where production and fluxes were generally higher. These

results certainly highlight the robustness of this approach for estimating basin-scale CH_4 production and flux pathways.

Meaning of maximum sediment production (*a*) and decay rate (*b*)

For a visualization of how CH_4 dynamics vary with depth and production, we fix the parameter b to 27.1 m^{-1} (i.e., approach 3b) while varying a (maximum production rate) and depth. The results of the exercise are shown as contours of bubble CH_4 content and ebullition pathway calculated as a function of depth and production (Fig. 10; calculations based on temperature and CH_4 profiles shown in Supporting Information Fig. S1). Note, that as parameter b is fixed as a constant, any variation of integrated sediment CH_4 production corresponds to a variation in parameter a (Prod = a/b). Figure 10 clearly shows that water depth majorly influences sediment CH_4 dynamics. This also demonstrates the tendency of reduced ebullition (or no ebullition) with increasing depth (West et al. 2016).We would like to point out that our theoretical contours of ebullition pathway look strikingly similar to the empirical contours of ebullition probability presented by West et al. (2016) in their Fig. 3.

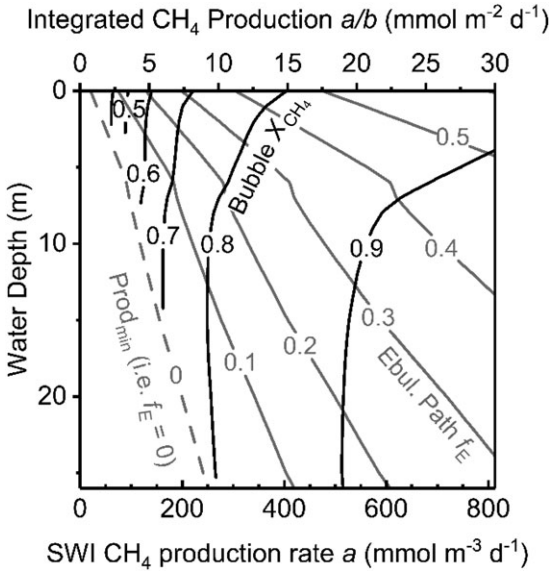

Fig. 10. Contour plot of bubble CH_4 content (Eq. 12) and CH_4 ebullition pathway (as a proportion of total CH_4 production; Eq. 11) with a constant sediment CH_4 production decay parameter b = 27.1 m^{-1} (Eq. 2). As in this case, b is fixed as a constant and variation in the integrated sediment CH_4 production corresponds to a variation in parameter a (Prod = a/b). Note also that the minimum CH_4 production necessary to sustain ebullition for a given parameter b increases approximately linearly with water depth.

The condition for the possibility of bubble formation (zero ebullition contour on Fig. 10) can be found algebraically from Eq. 4 by setting $z_{eb,min}$ to infinity (Bazhin 2010). Setting $z_{eb,min}$ to infinity, neglecting water vapor partial pressure and solving for parameter a, we obtain the critical minimum a (maximum CH_4 production; Eq. 2) for ebullition to occur for a given decay rate b (*see* Eq. 2).

$$a_{\min} = b^2 \cdot \frac{D_{CH_4}}{K_{CH_4}} \cdot \left(\rho g h + 0.22 \cdot P_{atm} - K_{H,CH_4} C_{CH_4,lake}\right) \qquad (14)$$

The minimum necessary integrated sediment CH_4 production rate for bubble formation is then consequently $Prod_{min} = a_{min}/b$. Both $Prod_{min}$ and a_{min} increase linearly with water depth for constant b, temperature, and lake CH_4 concentrations. In a real lake, however, the overlaying CH_4 concentration (discussed below) and temperature influence the value of $Prod_{min}$, although the linear contribution of water depth is dominant. This effect is visible in the almost linearly depth-dependent $Prod_{min}$ in Fig. 10.

Figure 11 shows the importance of a and b for the flux pathways. Here, we provide an example of model solutions using a fixed integrated production rate, i.e., we vary a in increments of 150 mmol m^{-3} d^{-1} and change in b to maintain a constant production rate of 15 mmol m^{-2} d^{-1}. The simulation was run for 5°C, 20 m water depth, and zero lake CH_4 concentration. We see that for this constant integrated CH_4

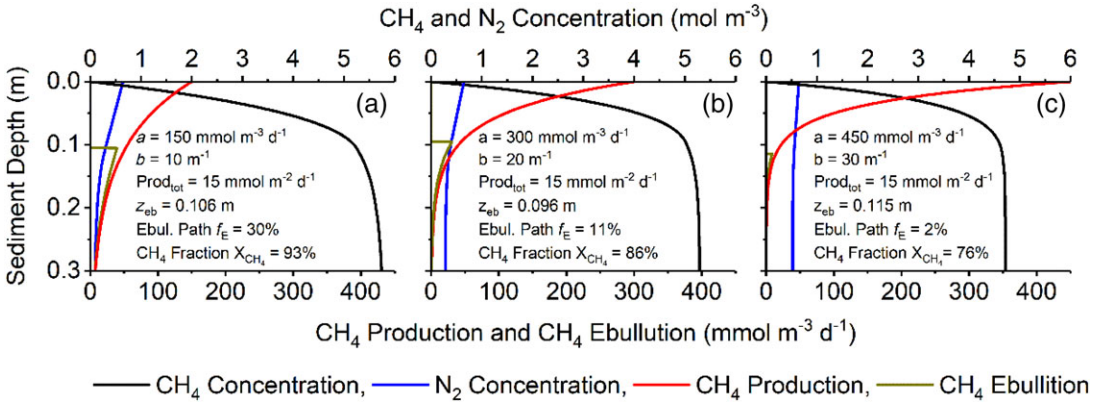

Fig. 11. Example sediment pore-water model calculations for 5°C at 20 m water depth. Three cases (**a**–**c**) with varying parameters a and b but same total CH_4 production.

production, the more rapidly the CH_4 production rate decays with sediment depth (i.e., high parameter *b*), the lower the maximum pore-water CH_4 concentration becomes, despite a higher *a*. Consequently, the CH_4 fraction in bubble gas and the CH_4 ebullition pathway are reduced as *a* and *b* increase.

Simplistically stated, for constant sedimentation rates and organic matter content, the parameters *a* and *b* in an exponential decaying sediment CH_4 production profile (Eq. 2) can be explained by the remineralization of the more labile organic matter over time due to methanogenesis following first-order kinetics. The parameters *a* and *b* would then reflect both the kinetics of methanogenesis and the sedimentation rate including the organic matter content and quality. We propose the relationship for sedimentation with constant organic matter input (quality) $a \propto k_1 \times C_{l,\ ini} \propto k_1 \times R_{PP}/w$, $b \propto k_1/w$, and Prod = $a/b \propto R_{PP}$, where k_1 is a first-order reaction constant, $C_{l,\ ini}$ reflects the initial concentration (at the SWI) of labile carbon source to be converted to CH_4, R_{PP} is the primary production, *w* is the sedimentation rate, and Prod is the integrated sediment CH_4 production.

Therefore, we come to a paradoxical conclusion that for a constant sedimentation rate and organic carbon input, the more refractory the carbon is (low k_1 within certain limits), the higher the CH_4 ebullition will likely be. Similarly, but not as counterintuitive, increasing the sedimentation rate (high *w*) of a constant labile carbon source would also lead to increased ebullition rates. This is in line with observations reported by Sobek et al. (2012) and Maeck et al. (2013). Of course other factors also affect ebullition, including depth, oxygen exposure, and temperature (Sobek et al. 2012).

Effect of overlying CH_4 water concentration on flux pathways

It is worth noting here that the analyses performed in this article used constant boundary conditions (temperature and overlying CH_4 concentration). CH_4 production is a function of temperature, and will therefore change when the overlying waters warm over the stratification season. This is especially important in shallow littoral systems where temperatures can increase substantially. Also important for the flux pathways—fraction emitted as either CH_4 diffusive or ebullitive flux—is the overlying CH_4 concentrations. As shown in Fig. 12 and assuming constant CH_4 production using the example from Fig. 11b, as the overlying water dissolved CH_4 concentration increases over time, the fraction emitted as diffusive fluxes will decrease and the ebullitive fraction will increase. As diffusive fluxes are a function of the concentration gradient at the SWI, increasing the overlying CH_4 concentration will decrease the concentration driving force, and thus the diffusive flux. Assuming a constant CH_4 production, this translates into a higher ebullitive flux. Thus, a remediation process, such as hypolimnetic oxygenation (McGinnis et al. 2004) could reduce ebullition by simply maintaining low hypolimnetic CH_4 concentrations.

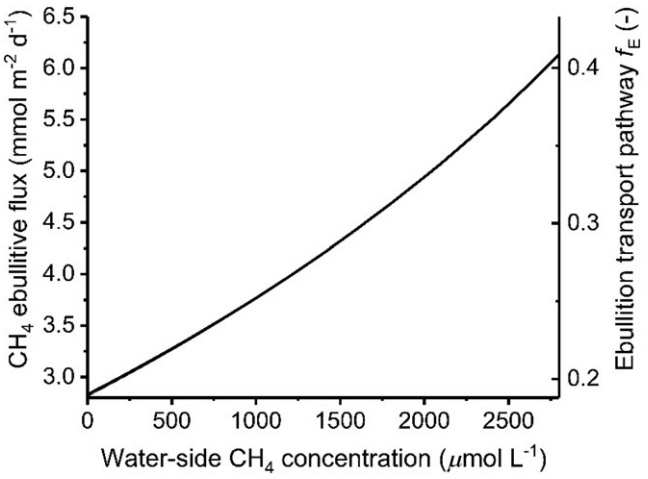

Fig. 12. Example calculation to show the effect of increasing CH_4 concentration in overlying water column on CH_4 ebullitive flux and fraction of production emitted as ebullition (ebullition transport pathway). Example calculated for same parameters *a* and *b*, temperature, and depth used for simulation in Fig. 11b.

Hotspots and intra-lake variability of CH_4 fluxes

Hotspots in terms of the relative value of CH_4 ebullition pathway can be detected based solely on the composition of sediment bubble gas as shown in Fig. 7. To quantify the CH_4 ebullition flux, however, one of the presented approaches must be applied to estimate the whole sediment CH_4 balance. This also helps to quantify the spatial variability of ebullition and diffusive CH_4 flux within a lake. To obtain a complete picture of basin-scale variability of CH_4 ebullition and diffusive fluxes, we propose to use a combination of several of the presented approaches when feasible. Any of the approaches combined with data collected at several point locations (e.g., bubble gas funnels) increases the robustness of basin-scale flux estimates.

Key assumptions and applicability to other waterbodies

The proposed model is applicable to other freshwaters where the same key assumptions apply: (1) the model conceptualization (Figs. 1, 3), (2) cohesive sediments (i.e., no advection), (3) negligible bioturbation, (4) exponential CH_4 production, (5) no N_2 production and N_2 concentration at the SWI is at atmospheric equilibrium. We discuss each of these assumptions below.

1. The model used in this study has been tested for validity both in the laboratory (Kusmin et al. 2006) and with a modeling study based on literature data (Bazhin 2010). Therefore, we assume that the basic conceptualization (two distinct layers) and impact on dissolved gas is applicable to many freshwater sediments. In its current form, it is a steady state model; therefore, the model represents averaged bubbling events (season scale) and lacks the resolution to resolve very short time scales.

2. The sediments are cohesive and we assume no advection. Advective transport arising from externally impressed flow (e.g., groundwater and near-bottom currents) is generally not present for muddy aquatic sediments because of their low permeabilities (Boudreau 1997). Advective transport arising from sedimentation and compaction can be neglected for the considered time and length scales (see e.g., Strassmann et al. 2005). The model is potentially applicable to permeable sediments with some modifications (McGinnis et al. 2014), however, more work is needed.
3. Bioturbation is not addressed explicitly, however, can be included simply by increasing the effective diffusion coefficient in the bioturbated zones. The inclusion of other types of bioturbation may need more modeling effort (Boudreau 1997).
4. We have applied an exponentially decaying CH_4 production assuming anoxic conditions. Numerically, it is straight forward to change the production profile $W(z)$ (Eq. 2) for any algebraic or numerical function (*see* Supporting Information section S10). For systems with oxic overlying water, we expect oxygen penetration in the top millimeters of the sediments (Bryant et al. 2010). We do not model CH_4 oxidation explicitly; however, the model formulation (Eq. 1) is still valid under these conditions. A possible formulation was presented by Wilkinson et al. (2015), who considered combined SWI effects with a sigmoid function. Such a general $W(z)$ could even be negative (net consumption) in the top parts. Finally, the laboratory results of Kusmin et al. (2006) and the model of Bazhin (2010) suggest that the model is applicable under oxic conditions.
5. We assume that N_2 production is negligible for the interpretation of our bubble gas composition samples below 13 m from June to December 2017. For the samples above 13 m, we cannot rule out the possibility of some influence due to denitrification. In lakes with high N_2 production in the sediments (for example, due to denitrification, anaerobic ammonium oxidation, or denitrifying anaerobic methane oxidation), both the approaches and the model used to estimate CH_4 emissions applied in this study would require additional parameterizations. The model itself can be modified to include N_2 production by including an N_2 production term or profile. As an example, we show model simulations using an exponentially decaying sediment N_2 production (Supporting Information Figs. S11 and S12). This adaption of our model would be applicable for the study of sediments where both denitrification and methanogenesis take place (Higgins et al. 2008).

Implications for CH_4 flux measurement methods

With approach 1, it is possible to close the sediment CH_4 mass balance at sites in the lake where funnel gas traps are deployed without any additional pore-water measurements; hence, approach 1 is already an improvement of the funnel gas trap method alone. Referring to Table 1 with possible combinations for estimation approaches, we can see that we can combine a measurement of total ebullition rate with, e.g., the measurement of diffusive flux CH_4 at SWI or sediment CH_4 production. This applies not only to the funnel gas trap method but also to hydroacoustic methods. Both methods rely for the calculation of CH_4 ebullition flux on the fraction of CH_4 in bubble gas, which is a priori not known but can be resolved for with a combination of any two parameters (Table 1).

Summary

We have confirmed the validity of measurement-modeling approaches with which it is possible to resolve the complete sediment CH_4 flux mass balance and basin-scale production and flux pathways. Measuring bubble gas composition alone already allows for resolving the relative proportion of the flux pathways at a given depth (i.e., diffusive versus ebullitive CH_4 fluxes) and identification of ebullition hotspots. Combining sediment bubble gas composition with additional measurements of ebullition flux at SWI (approach 1), depth of sediment bubble origin based on $\delta^{13}C_{CH_4}$ signature (approach 2), or sediment CH_4 production parameters a and b calibrated with approach 1 (approach 3a/3b) allows for solving the complete mass balance of CH_4 and flux pathways.

To summarize, approach 1 allows to close the sediment CH_4 mass balance at sites in the lake where funnel gas traps are deployed, without any additional pore-water measurements. Conversely, approach 2 is a novel way to estimate the entire sediment CH_4 mass balance, entirely independent from funnel gas trap measurements. Approach 2 is applicable to the whole lake but does require the measurement of $\delta^{13}C_{CH_4}$ signature in pore waters and bubble gas. Finally, if funnel gas traps are installed, approach 3 allows to quickly assess the CH_4 fluxes of the rest of the lake in cost-effective manner. All of these measurement approaches will allow better quantification of CH_4 ebullition and diffusion at SWI and integrated sediment CH_4 production.

For hypolimnetic CH_4 budgets based on evolution of CH_4 concentrations and knowledge of basin-scale diffusivity, Schmid et al. (2017) demonstrated that while the production rate of CH_4 can be estimated, the fractional contribution of ebullition could not be elucidated based on these data alone. Performing such a budget with the addition of sediment bubble gas composition, thus adding estimates of the flux pathways, would allow closing the CH_4 budget with higher certainty. In the case of Schmid et al. (2017), this could be relatively easily achieved by collecting data on sediment bubble gas composition at the various locations over time, following the recommendation for sampling frequency and locations of Wik et al. (2016). Such additional data would also improve the mass balance by accounting for spatial heterogeneity, and allow for accurate estimates of CH_4 bypassing the water column and emitted to the atmosphere via ebullition.

Current ebullitive CH_4 emission estimates from inland freshwaters are highly uncertain given their stochastic nature. Applying our approaches, combined with hypolimnetic CH_4 mass balances, will certainly allow the identification of CH_4 hotspots, better resolve in-lake CH_4 budgets, and improve overall CH_4 emission estimates from inland freshwaters and their contribution to global CH_4 budgets.

References

Bastviken, D., J. Cole, M. Pace, and L. Tranvik. 2004. Methane emissions from lakes: Dependence of lake characteristics, two regional assessments, and a global estimate. Global Biogeochem. Cycles **18**: GB4009. doi:10.1029/2004GB002238

Bastviken, D., L. J. Tranvik, J. A. Downing, P. M. Crill, and A. Enrich-Prast. 2011. Freshwater methane emissions offset the continental carbon sink. Science **331**: 50–50. doi:10.1126/science.1196808

Baulch, H. M., S. L. Schiff, R. Maranger, and P. J. Dillon. 2011. Nitrogen enrichment and the emission of nitrous oxide from streams. Global Biogeochem. Cycles **25**: GB4013. doi:10.1029/2011GB004047

Bazhin, N. M. 2003. Methane emission from bottom sediments. Chem. Sustain. Dev. **11**: 577–580. http://sibran.ru/upload/iblock/b1b/b1b83c2ba007f5d268ebc3322eca6a24.pdf

Bazhin, N. M. 2010. Theory of methane emission from wetlands. Energ. Environ. Sci. **3**: 1057. doi:10.1039/b923456j

Boudreau, B. P. 1997. Diagenetic models and their implementation: Modelling transport and reactions in aquatic sediments. Springer.

Boudreau, B. P. 2012. The physics of bubbles in surficial, soft, cohesive sediments. Mar. Pet. Geol. **38**: 1–18. doi:10.1016/j.marpetgeo.2012.07.002

Brennwald, M. S., R. Kipfer, and D. M. Imboden. 2005. Release of gas bubbles from lake sediment traced by noble gas isotopes in the sediment pore water. Earth Planet. Sci. Lett. **235**: 31–44. doi:10.1016/j.epsl.2005.03.004

Bryant, L. D., C. Lorrai, D. F. McGinnis, A. Brand, A. Wüest, and J. C. Little. 2010. Variable sediment oxygen uptake in response to dynamic forcing. Limnol. Oceanogr. **55**: 950–964. doi:10.4319/lo.2009.55.2.0950

Brennwald, M. S., M. Schmidt, J. Oser, and R. Kipfer. 2016. A portable and autonomous mass spectrometric system for on-site environmental gas analysis. Environ. Sci. Technol. **50**: 13455–13463. doi:10.1021/acs.est.6b03669

Buck, A. L. 1981. New equations for computing vapor pressure and enhancement factor. J. Appl. Meteorol. **20**: 1527–1532. doi:10.1175/1520-0450(1981)020<1527:NEFCVP>2.0.CO;2

Casper, P., S. C. Maberly, G. H. Hall, and B. J. Finlay. 2000. Fluxes of methane and carbon dioxide from a small productive lake to the atmosphere. Biogeochemistry **49**: 1–19. doi:10.1023/A:1006269900174

Chanton, J. P., C. S. Martens, and C. A. Kelley. 1989. Gas transport from methane-saturated, tidal freshwater and wetland sediments. Limnol. Oceanogr. **34**: 807–819. doi:10.4319/lo.1989.34.5.0807

Conrad, R. 2005. Quantification of methanogenic pathways using stable carbon isotopic signatures: a review and a proposal. Org. Geochem. **36**: 739–752. doi:10.1016/j.orggeochem.2004.09.006

D'Aoust, B. G. 2007. Technical note: Total dissolved gas pressure (TDGP) sensing in the laboratory. Dissolution Technol. **14**: 38–41. doi:10.14227/DT140207P38.

DelSontro, T., D. F. McGinnis, S. Sobek, I. Ostrovsky, and B. Wehrli. 2010. Extreme methane emissions from a swiss hydropower reservoir: Contribution from bubbling sediments. Environ. Sci. Technol. **44**: 2419–2425. doi:10.1021/es9031369

DelSontro, T., D. F. McGinnis, B. Wehrli, and I. Ostrovsky. 2015. Size does matter: Importance of large bubbles and small-scale hot spots for methane transport. Environ. Sci. Technol. **49**: 1268–1276. doi:10.1021/es5054286

Delwiche, K., S. Senft-Grupp, and H. Hemond. 2015. A novel optical sensor designed to measure methane bubble sizes in situ. Limnol. Oceanogr. Methods **13**: 712–721. doi:10.1002/lom3.10060

Dlugokencky, E. J., E. G. Nisbet, R. Fisher, and D. Lowry. 2011. Global atmospheric methane: Budget, changes and dangers. Philos. Trans. R. Soc. A Math. Phys. Eng. Sci. **369**: 2058–2072. doi:10.1098/rsta.2010.0341

Donis, D., S. Flury, A. Stöckli, J. E. Spangenberg, D. Vachon, and D. F. McGinnis. 2017. Full-scale evaluation of methane production under oxic conditions in a mesotrophic lake. Nat. Commun. **8**: 1661. doi:10.1038/s41467-017-01648-4. https://www.nature.com/articles/s41467-017-01648-4

Fischer, A. 1996. Isotopengeochemische Untersuchungen (d18O und d13C) im Wasser und in den Sedimenten des Soppensees (Kt. Luzern, Schweiz). Klimaveränderungen und Entwicklungsgeschichte des Sees seit dem Spätglazial. Swiss Federal Institute of Technology.

Flury, S., R. N. Glud, K. Premke, and D. F. McGinnis. 2015. Effect of sediment gas voids and ebullition on benthic solute exchange. Environ. Sci. Technol. **49**: 10413–10420. doi:10.1021/acs.est.5b01967

Higgins, T. M., J. H. McCutchan, and W. M. Lewis. 2008. Nitrogen ebullition in a Colorado plains river. Biogeochemistry **89**: 367–377. doi:10.1007/s10533-008-9225-4

Horn, C., P. Metzler, K. Ullrich, M. Koschorreck, and B. Boehrer. 2017. Methane storage and ebullition in monimolimnetic waters of polluted mine pit lake Vollert-sued, Germany. Sci. Total Environ. **584–585**: 1–10. doi:10.1016/j.scitotenv.2017.01.151

Jähne, B., G. Heinz, and W. Dietrich. 1987. Measurement of the diffusion coefficients of sparingly soluble gases in water. J. Geophys. Res. **92**: 10767. doi:10.1029/JC092iC10p10767

Joyce, J., and P. W. Jewell. 2003. Physical controls on methane ebullition from reservoirs and lakes. Environ. Eng. Geosci. **9**: 167–178. doi:10.2113/9.2.167

Katsman, R., I. Ostrovsky, and Y. Makovsky. 2013. Methane bubble growth in fine-grained muddy aquatic sediment: Insight from modeling. Earth Planet. Sci. Lett. **377–378**: 336–346. doi:10.1016/j.epsl.2013.07.011

Kipphut, G. W., and C. S. Martens. 1982. Biogeochemical cycling in an organic-rich coastal marine basin—3. Dissolved gas transport in methane-saturated sediments. Geochim. Cosmochim. Acta **46**: 2049–2060. doi:10.1016/0016-7037(82)90184-3

Kirschke, S., and others. 2013. Three decades of global methane sources and sinks. Nat. Geosci. **6**: 813–823. doi:10.1038/ngeo1955

Kusmin, A., N. M. Bazhin, and R. Conrad. 2006. Experimental test of a mechanistic model of production, flux and gas bubble zonation in non-vegetated flooded rice field soil. Biogeochemistry **78**: 315–342. doi:10.1007/s10533-005-4426-6

Liu, L., J. Wilkinson, K. Koca, C. Buchmann, and A. Lorke. 2016. The role of sediment structure in gas bubble storage and release. J. Geophys. Res. Biogeosci. **121**: 1992–2005. doi:10.1002/2016JG003456

Liu, L., and others. 2018. Methane bubble growth and migration in aquatic sediments observed by x-ray μCT. Environ. Sci. Tech. **52**: 2007–2015. doi:10.1021/acs.est.7b06061

Lotter, A. F. 1989. Evidence of annual layering in Holocene sediments of Soppensee, Switzerland. Aquat. Sci. **51**: 19–30. doi:10.1007/BF00877778

Lotter, A. F. 1991. Absolute dating of the late-glacial period in Switzerland using annually laminated sediments. Quatern. Res. **35**: 321–330. doi:10.1016/0033-5894(91)90048-A

Maeck, A., T. Delsontro, D. F. McGinnis, H. Fischer, S. Flury, M. Schmidt, P. Fietzek, and A. Lorke. 2013. Sediment trapping by dams creates methane emission hot spots. Environ. Sci. Technol. **47**: 8130–8137. doi:10.1021/es4003907

Martens, C. S., and R. A. Berner. 1977. Interstitial water chemistry of anoxic Long Island sound sediments. 1. Dissolved gases. Limnol. Oceanogr. **22**: 10–25. doi:10.4319/lo.1977.22.1.0010

Martens, C. S., D. B. Albert, and M. J. Alperin. 1998. Biogeochemical processes controlling methane in gassy coastal sediments—Part 1. A model coupling organic matter flux to gas production, oxidation and transport. Cont. Shelf Res. **18**: 1741–1770. doi:10.1016/S0278-4343(98)00056-9

McGinnis, D. F., A. Lorke, A. Wüest, A. Stöckli, and J. C. Little. 2004. Interaction between a bubble plume and the near field in a stratified lake. Water Resour. Res. **40**: W10206. doi:10.1029/2004WR003038

McGinnis, D. F., J. Greinert, Y. Artemov, S. E. Beaubien, and A. Wüest. 2006. Fate of rising methane bubbles in stratified waters: How much methane reaches the atmosphere? J. Geophys. Res. **111**: C09007. doi:10.1029/2005JC003183

McGinnis, D. F., S. Sommer, A. Lorke, R. N. Glud, and P. Linke. 2014. Quantifying tidally driven benthic oxygen exchange across permeable sediments: An aquatic eddy correlation study. J. Geophys. Res.: Ocean. **119**: 6918–6932. doi:10.1002/2014JC010303

Miyake, Y. 1951. The possibility and the allowable limit of formation of air bubbles in the sea. Pap. Meteorol. Geophys. **2**: 95–101. doi:10.2467/mripapers1950.2.1_95

Myhre, G., and others. 2013. Anthropogenic and natural radiative forcing. *In* T. F. Stocker and others [eds.], Climate change 2013: The physical science basis. Contribution of working group I to the fifth assessment report of the intergovernmental panel on climate change. Cambridge Univ. Press. pp. 659–740. doi:10.1017/CBO9781107415324.018

Natchimuthu, S., I. Sundgren, M. Gålfalk, L. Klemedtsson, P. Crill, Å. Danielsson, and D. Bastviken. 2016. Spatio-temporal variability of lake CH_4 fluxes and its influence on annual whole lake emission estimates. Limnol. Oceanogr. **61**: S13–S26. doi:10.1002/lno.10222

Nisbet, E. G., E. J. Dlugokencky, and P. Bousquet. 2014. Methane on the rise—again. Science **343**: 493–495. doi:10.1126/science.1247828

Nozhevnikova, A. N., V. Nekrasova, A. Ammann, A. J. B. Zehnder, B. Wehrli, and C. Holliger. 2007. Influence of temperature and high acetate concentrations on methanogenensis in lake sediment slurries. FEMS Microbiol. Ecol. **62**: 336–344. doi:10.1111/j.1574-6941.2007.00389.x

Ostrovsky, I., D. F. McGinnis, L. Lapidus, and W. Eckert. 2008. Quantifying gas ebullition with echosounder: The role of methane transport by bubbles in a medium-sized lake. Limnol. Oceanogr. Methods **6**: 105–118. doi:10.4319/lom.2008.6.105

Popp, T. J., J. P. Chanton, G. J. Whiting, and N. Grant. 2000. Evaluation of methane oxidation in the rhizosphere of a Carex dominated fen in north Central Alberta. Can. Biogeochem. **51**: 259–281. doi:10.1023/A:1006452609284

Reeburgh, W. S. 1969. Observations of gases in the Chesapeake bay sediments. Limnol. Oceanogr. **14**: 368–375. doi:10.4319/lo.1969.14.3.0368

Sander, R. 2015. Compilation of Henry's law constants (version 4.0) for water as solvent. Atmos. Chem. Phys. **15**: 4399–4981. doi:10.5194/acp-15-4399-2015

Scandella, B. P., L. Pillsbury, T. Weber, C. Ruppel, H. F. Hemond, and R. Juanes. 2016. Ephemerality of discrete methane vents in lake sediments. Geophys. Res. Lett. **43**: 4374–4381. doi:10.1002/2016GL068668

Schmid, M., I. Ostrovsky, and D. F. McGinnis. 2017. Role of gas ebullition in the methane budget of a deep subtropical lake: What can we learn from process-based modeling? Limnol. Oceanogr. **62**: 2674–2698. doi:10.1002/lno.10598

Schulz, S., and R. Conrad. 1995. Effect of algal deposition on acetate and methane concentrations in the profundal sediment of a deep lake (Lake Constance). FEMS Microb. Ecol. **16**: 251–260. doi:10.1111/j.1574-6941.1995.tb00289.x

Sobek, S., T. DelSontro, N. Wongfun, and B. Wehrli. 2012. Extreme organic carbon burial fuels intense methane bubbling in a temperate reservoir. Geophys. Res. Lett. **39**: L01401. doi:10.1029/2011GL050144

Strassmann, K. M., M. S. Brennwald, F. Peeters, and R. Kipfer. 2005. Dissolved noble gases in the porewater of lacustrine

sediments as palaeolimnological proxies. Geochim. Cosmochim. Acta **69**: 1665–1674. doi:10.1016/j.gca.2004.07.037

Turner, A. J., C. Frankenberg, P. O. Wennberg, and D. J. Jacob. 2017. Ambiguity in the causes for decadal trends in atmospheric methane and hydroxyl. Proc. Natl. Acad. Sci. USA **114**: 5367–5372. doi:10.1073/pnas.1616020114

Walter, K. M., J. P. Chanton, F. S. Chapin, E. A. G. Schuur, and S. A. Zimov. 2008. Methane production and bubble emissions from arctic lakes: Isotopic implications for source pathways and ages. J. Geophys. Res. **113**: G00A08. doi:10.1029/2007JG000569

West, W. E., K. P. Creamer, and S. E. Jones. 2016. Productivity and depth regulate lake contributions to atmospheric methane. Limnol. Oceanogr. **61**: S51–S61. doi:10.1002/lno.10247

Wik, M., B. F. Thornton, D. Bastviken, J. Uhlbäck, and P. M. Crill. 2016. Biased sampling of methane release from northern lakes: A problem for extrapolation. Geophys. Res. Lett. **43**: 1256–1262. doi:10.1002/2015GL066501

Wilkinson, J., A. Maeck, Z. Alshboul, and A. Lorke. 2015. Continuous Seasonal River ebullition measurements linked to sediment methane formation. Environ. Sci. Technol. **49**: 13121–13129. doi:10.1021/acs.est.5b01525

Worden, J. R., A. A. Bloom, S. Pandey, Z. Jiang, H. M. Worden, T. W. Walker, S. Houweling, and T. Röckmann. 2017. Reduced biomass burning emissions reconcile conflicting estimates of the post-2006 atmospheric methane budget. Nat. Commun. **8**: 2227. doi:10.1038/s41467-017-02246-0

Wuebbles, D., and K. Hayhoe. 2002. Atmospheric methane and global change. Earth-Sci. Rev. **57**: 177–210. doi:10.1016/S0012-8252(01)00062-9

Yvon-Durocher, G., A. P. Allen, D. Bastviken, R. Conrad, C. Gudasz, A. St-Pierre, N. Thanh-Duc, and P. A. del Giorgio. 2014. Methane fluxes show consistent temperature dependence across microbial to ecosystem scales. Nature **507**: 488–491. doi:10.1038/nature13164

Zepp Falz, K., C. Holliger, R. Großkopf, W. Liesack, A. N. Nozhevnikova, B. Müller, B. Wehrli, and D. Hahn. 1999. Vertical distribution of methanogens in the anoxic sediment of Rotsee (Switzerland). Appl. Environ. Microbiol. **65**: 2402–2408.

Acknowledgments

The authors would like to thank Sabine Flury for help with field work and Jeremey Wilkinson and Andreas Lorke from the University of Koblenz-Landau for advice and support for laboratory incubations. The authors further thank Matthias Brennwald and Rolf Kipfer from Eawag Dübendorf for their support in assembly and operation of a field portable mass spectrometer and use of their stable isotope analyzer. Thanks to Peter Feldens from the Leibniz-Institute for Baltic Sea Research for hydroacoustic bathymetry mapping and Gilles Vilmart from the CAMAS Consulting platform at University of Geneva for advice on the formulation of the numerical model. The authors thank Bernhard Pfyffer for his kind support of this study on Lake Soppen, and access to the infrastructure. Thanks to César Ordóñez and Tonya DelSontro for their input on earlier versions of this manuscript. This study was funded by the Swiss National Science Foundation (Grant 200021_160018, Bubble Flux).

Conflict of Interest:

None declared.

Submitted 14 May 2018
Revised 23 November 2018
Accepted 14 January 2019

Associate editor: Kimberly Wickland